NASA Technical Memorandum 108866

Simulation Model of the Integrated Flight/Propulsion Control System, Displays, and Propulsion System for an ASTOVL Lift-Fan Aircraft

William W. Y. Chung, Paul F. Borchers, and James A. Franklin
Ames Research Center, Moffett Field, California

April 1995

National Aeronautics and
Space Administration

Ames Research Center
Moffett Field, California 94035-1000

NOMENCLATURE

APP	approach control mode
ATM	automatic transition control sub-mode
CTO	cruise/takeoff control mode
FTM	full thrust command control sub-mode
HUD	head-up display
IAS	indicated airspeed
IGV	inlet guide vane
LFI	lift-fan inlet
MTV	manual thrust vector control mode
RCS	reaction control system
SCAS	stability and command augmentation system
STOVL	short takeoff and vertical landing
TRC	translational rate command control mode
V/STOL	vertical or short takeoff and landing
wow	weight on wheels
α_c	commanded angle of attack, radians
ΔM	aerodynamic pitching moment that propulsion system counteracts, ft-lb
ΔX	body x-axis force that SCAS commands, lb
ΔZ	body z-axis force that SCAS commands, lb
γ_q	quickened flightpath angle for HUD, deg
δ_A	aileron deflection, deg
δ_C	canard deflection, deg

δ_{CN}	cruise-nozzle deflection angle, deg
δ_{LF_x}	longitudinal deflection angle of the lift-fan nozzle, deg
δ_{LF_y}	lateral deflection angle of the lift-fan nozzle, deg
δ_{LN}	lift-nozzle deflection angle prior to yaw axis command additions, deg
δ_{LLN}	left lift-nozzle deflection angle, deg
δ_{long}	longitudinal stick deflection, inches
δ_{neu}	cruise-nozzle deflection angle that produces no pitching moment
δ_{PRCS}	reaction control system pitch thrust, lb
δ_R	rudder deflection, deg
δ_{RLN}	right lift-nozzle deflection angle, deg
δ_{RRCS}	reaction control system roll thrust, lb
δ_T, δ_{th}	throttle position, deg
δ_{YRCS}	reaction control system yaw thrust, lb
ϕ	bank angle, radians
η_{CN}	cruise-nozzle efficiency factor
η_{LF}	lift-fan nozzle efficiency factor
η_{LN}	lift-nozzle efficiency factor
θ_N, θ_j	net thrust vector angle, deg
θ_s, θ_c	commanded pitch attitude, radians
ω_{core}	core (lift/cruise) engine bandwidth, rad/sec
$\bar{c}$	mean aerodynamic chord, ft
$C_{m_{GE}}$	pitching moment coefficient due to ground effect
C_{m_o}	pitching moment coefficient at zero angle of attack

C_{m_α}	pitching moment coefficient due to angle of attack, 1/rad
D	aerodynamic drag, lb
F_{AI_x}	auxiliary inlet force in body axis x-direction, lb
F_{AI_z}	auxiliary inlet force in body axis z-direction, lb
F_{CN_x}	cruise-nozzle force in body axis x-direction, lb
F_{CN_z}	cruise-nozzle force in body axis z-direction, lb
F_{EX}	total propulsion system force in body axis x-direction, lb
F_{EY}	total propulsion system force in body axis y-direction, lb
F_{EZ}	total propulsion system force in body axis z-direction, lb
F_{LF_x}	lift-fan force in body axis, x-direction, lb
F_{LLN_x}	left lift-nozzle force in body axis, x-direction, lb
F_{LN_x}	lift-nozzle force in body axis x-direction, lb
F_{LN_z}	lift-nozzle force in body axis z-direction, lb
F_{PI_x}	primary inlet force in body axis x-direction, lb
F_{PI_z}	primary inlet force in body axis z-direction, lb
F_{RLN_x}	right lift-nozzle force in body axis, x-direction, lb
g	acceleration due to gravity, ft/sec^2
$\dot{h}$	vertical velocity, ft/sec
K	control system gain
K_{AUG}	augmentation ratio of the lift fan
l_{CN}	distance from cruise nozzle to center of gravity, ft
L	aerodynamic lift, lb
L_{CN}	cruise-nozzle moment arm, ft

L_{LF}	lift-fan moment arm, ft
L_{LN}	lift-nozzle moment arm, ft
MGE_{LF}	factor to modify jet-induced pitching moment, scaled to lift-fan thrust
MGE_{LN}	factor to modify jet-induced pitching moment, scaled to lift-nozzle thrust
m	aircraft mass, slugs
$\dot{m}_{AI}$	mass flow rate, auxiliary inlet, lbm/sec
$\dot{m}_e$	engine mass flow rate, slugs/sec
$\dot{m}_{LF}$	mass flow rate, lift fan, lbm/sec
$\dot{m}_{PI}$	mass flow rate, primary inlet, lbm/sec
P_B	aircraft roll rate in body axis, rad/sec
Q_B	aircraft pitch rate in body axis, rad/sec
$\bar{q}$	dynamic pressure, lb/ft^2
R_B	aircraft yaw rate in body axis, rad/sec
S	reference wing area, ft^2
$Slope_L$	lower command scaling slope for the throttle, authority/percent of throttle travel
$Slope_u$	upper command scaling slope for the throttle, authority/percent of throttle travel
T_{CN}	cruise-nozzle thrust, lb
$T_{CN_{CMD}}$	cruise-nozzle thrust command, lb
T_{CN1}	cruise-nozzle thrust prior to modification for axial commands, lb
T_{EL}	total propulsion system rolling moment, ft-lb
T_{EM}	total propulsion system pitching moment, ft-lb
T_{EN}	total propulsion system yawing moment, ft-lb
TGE_{LF}	factor to modify lift-fan thrust in ground effect

TGE_{LN}	factor to modify lift-nozzle thrust in ground effect
T_{LF}	total lift-fan thrust, lb
T_{LF_F}	lift-fan thrust due to inlet guide vane authority, lb
T_{LF_S}	lift-fan thrust due to fan inertia response, lb
T_{LF1}	lift-fan thrust prior to modification for axial commands, lb
$T_{LF_{CMD}}$	lift-fan thrust command, lb
T_{LLN}	left lift-nozzle thrust, lb
$T_{LLN_{CMD}}$	left lift-nozzle thrust command, lb
T_{LN1}	lift-nozzle thrust commanded prior to axial command additions
T_{RLN}	right lift-nozzle thrust, lb
$T_{RLN_{CMD}}$	right lift-nozzle thrust command, lb
$T_{T_{CMD}}$	total core (lift/cruise) engine thrust commanded, lb
T_{TOT}	total core (lift/cruise) engine thrust, lb
$T_{T_{Ref}}$	referenced lift/cruise engine steady state thrust, lb
U_B	aircraft velocity in body axis, x-direction, ft/sec
V_{af}	filtered airspeed, ft/sec
V_B	aircraft velocity in body axis, y-direction, ft/sec
V_x	x-axis groundspeed, ft/sec
V_T	true airspeed, ft/sec
W	aircraft weight, lb
W_B	aircraft velocity in body axis, z-direction, ft/sec
x_{CN}	longitudinal distance from cruise nozzle to aircraft center of gravity, ft
x_{LF}	longitudinal distance from lift-fan nozzle to aircraft center of gravity, ft

x_{LN}	longitudinal distance from lift nozzle to aircraft center of gravity, ft
y_{LN}	lateral distance from lift nozzle to aircraft center of gravity, ft
z_{CN}	vertical distance from cruise nozzle to aircraft center of gravity, ft
z_{LF}	vertical distance from lift-fan nozzle to aircraft center of gravity, ft
z_{LN}	vertical distance from lift nozzle to aircraft center of gravity, ft

Simulation Model of the Integrated Flight/Propulsion Control System, Displays, and Propulsion System for an ASTOVL Lift-Fan Aircraft

William W. Y. Chung, Paul F. Borchers, and James A. Franklin

Ames Research Center

SUMMARY

A simulation model has been developed for use in piloted evaluations of takeoff, transition, hover, and landing characteristics of an advanced, short takeoff, vertical landing lift-fan fighter aircraft. The flight/propulsion control system includes modes for several response types which are coupled to the aircraft's aerodynamic and propulsion system effectors through a control selector tailored to the lift-fan propulsion system. Head-up display modes for approach and hover, tailored to their corresponding control modes are provided in the simulation. Propulsion system components modeled include a remote lift fan and a lift/cruise engine. Their static performance and dynamic response are represented by the model. A separate report describes the subsonic, power-off aerodynamics and jet induced aerodynamics in hover and forward flight, including ground effects.

INTRODUCTION

NASA Ames Research Center is participating in technology development for advanced short takeoff vertical landing (ASTOVL) fighter aircraft as a member of the Advanced Research Projects Agency (ARPA) ASTOVL program. Integration of flight and propulsion controls is one of the critical technologies being pursued in that program. NASA's role in the program is to participate in developing design guidelines for integrated flight/propulsion controls, support ARPA technology development for ASTOVL demonstrator aircraft, and provide consultation on integrated control design to ARPA contractors. This work will be accomplished in a joint program with ARPA, Department of Defense agencies, US and UK industry, and the UK Ministry of Defence. Specifically, NASA will carry out design guideline analyses for the control system and conduct piloted simulations on the Ames Research Center Vertical Motion Simulator (VMS) to evaluate design guidelines and to assess the merits of contending design approaches.

The initial effort in this program has been to develop a mathematical model for simulation of a representative ASTOVL aircraft concept. This simulation development has followed the approach employed in previous STOVL aircraft simulation models, an example of which is provided in reference 1. Representation of the aircraft's aerodynamic characteristics are presented in reference 2. This report describes the aircraft's integrated flight/propulsion control system and head-up display and the propulsion system performance and dynamic response. This simulation model has been used in an experiment on the VMS to gain initial experience with control system behavior and flying qualities for this aircraft concept.

Description of the Lift-Fan STOVL Aircraft

The lift-fan STOVL aircraft is a single-place, single-engine fighter/attack aircraft, shown in figure 1, featuring a wing-canard arrangement with twin vertical tails. Geometric characteristics of the configuration are summarized in table 1; mass properties are specified in table 2.

The propulsion system concept is presented in figure 2. It consists of a remote lift fan coupled to a lift/cruise turbofan engine to permit continuous transfer of energy from the lift/cruise engine to the lift fan. Further, the lift/cruise engine exhaust is either ducted aft to a thrust deflecting cruise nozzle in conventional flight or diverted to two deflecting lift nozzles in vertical flight. Throughout transition, flow can be continuously transferred between the cruise and lift nozzles. Lift fan and lift-nozzle thrust can be deflected downwards from 45 to 100 deg relative to the aircraft waterline. The cruise nozzle can be deflected ±20 deg from the vertical.

The basic flight-control system consists of the canard, ailerons and twin rudders for aerodynamic effectors during forward flight. For powered-lift operation, control is provided by differential thrust transfer between the lift fan and lift nozzles, deflection of lift-fan and lift-nozzle thrust, and deflection of cruise-nozzle thrust. Pitch control is achieved by a combination of canard deflection, thrust transfer between the lift fan and lift nozzles, and deflection of the cruise nozzle. Roll control is produced by the ailerons and differential thrust transfer between the lift nozzles. Yaw control is derived from the combination of rudder deflection, differential lift-nozzle deflection, and lateral lift-fan thrust deflection. As an option, reaction control, powered by engine compressor bleed air, can provide additional control moments through nozzles located in the wing extremities and in the tail. Longitudinal acceleration is achieved through thrust transfer between the lift fan, lift nozzles and cruise nozzles and by deflection of the lift-fan and lift-nozzle thrust. The integrated flight/propulsion control system must coordinate all of these aerodynamic and propulsive control effectors so that, from the pilot's perspective, the aircraft consistently responds to cockpit inceptor inputs, whether in airborne or jetborne flight.

Integrated Flight/Propulsion Control System

The flight/propulsion control system model follows the structure shown in figure 3. It includes the pilot's command inputs, the regulator that acts on the pilot's commands and sensed aircraft and propulsion system state variables, and the control selector that couples these commands to the appropriate aerodynamic or propulsion control effectors. The pilot's commands and regulator are subdivided corresponding to pitch, roll, and yaw attitude controls, and vertical, longitudinal, and lateral translational velocity controls. Within each of these, the different command modes shown in table 3 may be obtained depending on the phase of flight and the pilot's task. Descriptions of these modes follow, presented in order of increasing system complexity.

In the cruise/takeoff (CTO) mode, the pilot has direct control of the magnitude of the lift/cruise engine thrust. The propulsive lift system is not in use, and the pilot has no direct control of the thrust

vector angle. Rate damping augmentation is provided for pitch and roll control along with dutch roll damping and turn coordination for the yaw axis.

The manual thrust vector (MTV) mode allows the pilot to control the magnitude of the propulsion system thrust (lift-fan plus lift/cruise engine thrust) as well as the direction of the net thrust vector. No feedback control loops are used for either speed or flightpath control. Pitch and roll are controlled through rate command/attitude hold augmentation in transition, blending to attitude command/attitude hold at low speed. Yaw control is the same as for CTO at higher airspeeds during transition, and then blends to yaw rate command at low speed.

The approach (APP) mode activates a longitudinal acceleration command/velocity hold system, with the net thrust vector angle as the speed control effector. In decelerating from wingborne to powered lift flight, a flightpath control system is activated as the net thrust vector angle exceeds 70 deg and the commanded core engine thrust exceeds 70 percent of its maximum value. This flightpath system remains activated until the net thrust vector angle decreases below 50 deg. The portion of the APP mode that does not use a flightpath controller is called full thrust mode (FTM), as the pilot still has direct control of the cruise engine thrust, while that portion that uses a flightpath controller is called automatic transition mode (ATM). Pitch, roll, and yaw control are identical to that for MTV.

Lastly, the translational rate command (TRC) mode is reserved exclusively for the low-speed powered lift and hover flight regime. Propulsion system control in this mode consists of a vertical velocity and a longitudinal velocity control system. The control system uses roll attitude to provide the pilot with direct command of lateral velocity. The yaw axis control remains the same as that for MTV.

Control mode availability is subject to the restrictions shown in figure 4. Assuming the lift fan and its inlet/exhaust mechanical components have a 250 knot airspeed operational limit, CTO is the only mode available for this and higher airspeeds. The pilot engages the lift fan by selecting MTV or APP when the airspeed is between 250 and 150 knots; if the lift fan is not engaged by the time the airspeed drops below 150 knots, then a landing in CTO mode is required, or the pilot must wave off and start the approach again. TRC cannot be selected until the airspeed has dropped below 60 knots, nor can TRC be used to command an airspeed greater than this value. Upon a landing following jetborne flight, the flight control mode automatically reverts to MTV, disengaging the vertical velocity control system. It follows that MTV is the only fan-engaged mode used for vertical and short takeoff as it provides the pilot with direct control of the thrust vector. The CTO mode can also be selected while the aircraft is on the ground, allowing for conventional takeoff. The lift fan will be shut down automatically in flight if the airspeed exceeds 250 knots; the pilot can manually disengage the lift fan by selecting CTO mode, but this option is only available if the net thrust vector angle is directed fully aft . This feature prevents the pilot from disengaging the lift fan while the fan is still providing significant propulsive lift for the aircraft. Lastly, the MTV mode can be selected any time the lift fan is engaged by depressing a button on the nozzle lever. This button disengages the clutch that backdrives the thrust vector handle and allows the pilot to manually direct the thrust vector, providing a rapid acceleration or waveoff capability.

The material which follows first describes the pilot command inputs and regulator laws for each of the six control axes, and then presents the control selector.

Command and Regulator Models

Pitch control– The pitch attitude control modes for transition and hover are a direct application of the state-rate feedback implicit-model following system that has been evaluated on a number of V/STOL aircraft simulations at Ames Research Center, including the AV-8 Harrier and the E-7A and Mixed Flow Vectored Thrust STOVL aircraft. Its structure is shown in figure 5. The pilot's inputs come through the control stick and trim switch. Either attitude-command/attitude hold or rate-command/attitude hold modes can be implemented, depending on whether the gain K_{111} is zero or not. Rate-command/attitude hold is blended to attitude-command/attitude hold below 70 knots by ramping K_{111} between its nominal value and zero over the speed range from 70 to 60 knots. Gain K_{222} establishes control sensitivity for attitude command; K_{111} serves the same purpose for the rate command mode while K_{222} is used to adjust overshoot in pitch response. Proportional-plus-integral control in the forward path is obtained from the positive feedback of the pitch command through the first order lag defined by τ_9. The value of the lag time constant was set to approximate the lag of the pitch control actuator. Gain K_{FB} blends feedback variables between body angular rate and Euler axis sensors depending on flap position (K_{FB} = 0 flaps up; 1 flaps down).

The combination of angular acceleration feedback and proportional plus integral control produces a very robust system to variations in aircraft configuration and flight condition. Angular acceleration provides sufficient lead compensation to restore stability margins that are eroded by the integral control, while still maintaining the closed-loop gain to achieve the specified control bandwidth as well as good command tracking and disturbance rejection. As noted in table 4 only the final forward loop gain (K_{300}) is changed in proportion to variations in sensitivity of the control effectors over the transition and hover envelope. Otherwise, the gains are virtually the same as those used for the Harrier. Integrator limiting is imposed when the pitch control effectors reach the limit of their effectiveness or are rate saturated. Attitude stabilization is synchronized and integral control is removed when the aircraft is on the ground (wow on).

Roll control– Roll control modes are presented in figure 6. Rate-command/attitude hold or attitude-command/attitude hold modes are produced with the same form of control laws as for pitch. The control stick and trim switch provide the pilot's inputs, and the control gains and limiting logic are completely analogous to those for pitch. As was the case for pitch control, rate-command/attitude -hold is blended to attitude-command/attitude-hold, in this case by ramping K_{333} from its nominal value to zero over the speed range from 50 to 40 knots. Gain K_1 establishes control sensitivity for attitude command; K_{333} serves this purpose for the rate command mode while K_1 is used to adjust overshoot in pitch response. Lateral velocity control is accomplished through appropriate commands to the roll control. Switch C in figure 6 is activated by mode control to select either roll command or lateral velocity command through the control stick for hover operations. Gain K_6 sets the control sensitivity, $K_{\phi 2}$, K_9, and the equalization transfer function provide the desired control bandwidth and associated roll response to the pilot's velocity command inputs. The forward loop gain K_3 is adjusted in proportion to variation in control sensitivity. Proportional-plus-integral control were achieved as for the pitch control with the positive feedback of the lagged roll control command, where τ_8 approximates the roll control actuator lag. Again, K_{FB} blends body angular rate and Euler axis

feedbacks depending on flap position. Attitude stabilization and integral control are removed on the ground.

Yaw control– Yaw control modes (fig. 7) provide sideslip command during transition and blend to yaw rate command at low speed and in hover. The gain K_B provides a linear blend between the two modes over the speed range from 50 to 40 knots. The yaw control command is produced by the difference between the commanded yaw acceleration and the yaw acceleration produced by the basic aircraft's yaw response characteristics. In forward flight the commanded acceleration is produced by a second order dutch roll model derived from measured sideslip and sideslip rate, where the sideslip feedback gain is chosen to set dutch roll frequency and the sideslip rate gain establishes dutch roll damping. During low speed and hover, the same state-rate feedback structure as employed for pitch and roll control is used for yaw rate command, including angular acceleration feedback and proportional plus integral feed forward. Feedback of sideslip, roll rate, yaw rate, and lateral control position, in conjunction with the model of the known nonlinear directional aerodynamic characteristics, define the contribution of the basic aircraft to yaw acceleration.

Flightpath and velocity control– The flightpath and velocity control modes use a combination of the state-rate feedback concept along with the nonlinear-inverse system design which has been investigated in flight on the NASA Quiet Short Haul Research Aircraft (QSRA) (ref. 3) and several STOVL flight simulations which include the E-7A (ref. 4) and Mixed Flow Vectored Thrust STOVL aircraft (ref. 5). The same design method also has been investigated in the E-7D flight simulation (ref. 6) which included a detailed component level propulsion system. The state-rate feedback portion of the flightpath and velocity control is used to generate acceleration commands to the nonlinear inverse system when an advanced augmentation mode, i.e., APP or TRC, is engaged.

The flightpath angle or vertical velocity command (fig. 8) is controlled by the throttle. This command input, in combination with the vertical velocity and normal acceleration feedbacks, produces the vertical acceleration command, $\ddot{z}_{cmd}$. The implicit proportional-plus-integral feed forward is employed in the forward loop to achieve good model following response and noise rejection. None of the gains vary throughout transition or in hover. The velocity V_x is ground speed along track and is used to convert the pilot's flightpath angle command to an equivalent vertical velocity command. For groundspeeds below 60 knots, this velocity is frozen at the 60-knot value to convert the pilot's command from flightpath angle to vertical velocity as is appropriate for hover and low speed flight. Switch G is closed when either APP or TRC is engaged. ATM in the acceleration feedback path is a second order transfer function with a damping ratio of 0.707 and a natural frequency of 5 rad/sec to provide a smooth transition when either flightpath command loop or vertical speed command loop is engaged. Switch F is closed in TRC to allow an altitude hold response for precision hover. When it is engaged, the reference altitude h_{prime} is synchronized with the measured radar altitude until the pilot's vertical velocity command is centered, at which time the reference altitude is held at the past value.

The longitudinal velocity control shown in figure 9 produces axial acceleration commands, $\ddot{x}_{cmd}$, with a control structure similar to that for vertical velocity. During transition between forward flight and hover, the pilot commands the longitudinal acceleration using a thumbwheel on the control stick. This mode is selected by engaging APP mode, Switch E. Longitudinal acceleration and groundspeed combine with the pilot's commands and proportional-plus-integral feed forward to complete the

implicit state rate feedback model following design. All the gains in this control loop remain constant. For precision hover, the thumbwheel is switched out in TRC mode, Switch F, and the control stick provides longitudinal velocity commands. In this mode, the stick is disconnected from the pitch attitude command system. While most of the hover maneuvering is performed at a constant pitch attitude, attitude changes can be made through use of the trim switch shown in figure 5.

In CTO mode, the throttle directly controls the core engine's RPM and total thrust magnitude, figure 8. In MTV, a nozzle lever controller is used to control the thrust vector angle. The total thrust command, which is set by the throttle, and the thrust vector angle command, which is set by the nozzle lever, are sent to the thrust management system to calculate each nozzle thrust command and deflection.

When either APP or TRC is engaged, the commands for thrust and deflection of each nozzle are derived from longitudinal acceleration command, $\ddot{x}_{cmd}$, vertical acceleration command, $\ddot{z}_{cmd}$, (both in flightpath inertia axes), and pitch acceleration command, $\dot{q}_{cmd}$. To convert these acceleration commands to each nozzle's thrust and deflection commands, the axial and vertical components of the required total thrust from the propulsion system are calculated. These forces, ΔX and ΔZ, are calculated based on the aerodynamic lift and drag forces, aircraft attitudes, inlet forces, weight of the aircraft, and translational acceleration commands (eqs. 1 and 2).

$$\Delta X = m\ddot{x}_{cmd}\cos\theta_s - m\ddot{z}_{cmd}\sin\theta_s + D\cos\alpha_c - L\sin\alpha_c\cos\phi + W\sin\theta_s - F_{PIX} - F_{AIX} \quad (1)$$

$$\Delta Z = \frac{m\ddot{x}_{cmd}\sin\theta_s + m\ddot{z}_{cmd}\cos\theta_s + D\sin\alpha_c - W\cos\theta_s}{\cos\phi} + L\cos\alpha_c - F_{PIZ} - F_{AIZ} \quad (2)$$

APP has two sub-modes, the full thrust mode (FTM) and the automatic thrust mode (ATM). In APP/FTM, throttle commands total thrust and thumb-wheel commands flightpath acceleration command, $\ddot{x}_{cmd}$. In APP/ATM, the throttle controller is converted to flightpath command, γ_{cmd}, at speeds higher than 60 knots, and to vertical velocity command, $\dot{h}_{cmd}$, at speeds lower than 60 knots. The switch from APP/FTM to APP/ATM occurs when the thrust vector angle is greater than 70 deg and the throttle setting is greater than 60 percent. Reversion APP/ATM to APP/FTM occurs when the thrust vector angle is less than 50 deg and is independent to the throttle setting.

Since in APP/FTM, pilot controls $\ddot{x}_{cmd}$ with the thumbwheel controller, and altitude with pitch attitude, the vertical acceleration command, $\ddot{z}_{cmd}$, and the output of the first order filter, with the time constant of τ_{CNT} in figure 8, in the vertical acceleration command loop, are all set to zero. $\ddot{z}_{cmd}$ and the output of the first order filter are initialized to the flightpath angle command, γ_{cmd}, at the time when transitioning from APP/FTM to APP/ATM as shown in equation 3.

$$\ddot{z}_{cmd} = -\frac{\Delta X - m\ddot{x}_{cmd}\cos\theta_s - D\cos\alpha_c + L\sin\alpha_c\cos\phi - W\sin\theta_s + F_{PIX} + F_{AIX}}{m\sin\theta_s} \quad (3)$$

θ_s, in equation 1, is the pitch attitude command from the attitude command loop in flightpath command mode, and is controlled by the longitudinal stick, δ_{long}, and the pitch trim switch. In

flightpath command mode, pitch response is decoupled from the flightpath command and longitudinal speed command. To provide the capability of controlling longitudinal speed with pitch attitude in APP mode, the flightpath command and speed control loops have to be disabled. This is done by disconnecting θ_s from pitch attitude control, δ_{long}, when the longitudinal speed control, i.e., thumb-wheel, is in detent and ground speed is less than 60 knots. This effectively converts $\ddot{x}_{cmd}$ and $\ddot{z}_{cmd}$ from the inertia coordinate system to an axes system following the body axis with an angle defined by θ_s. As a consequence, the pitch and speed coupling is introduced. The input from the pitch trim rate switch to θ_s remains active to give pilot control over this new axes system with respect to the body axes as well as the pitch attitude in this control configuration. The flightpath command and speed control mode is restored whenever pilot rolls the thumb-wheel out of detent.

The throttle controller commands total thrust magnitude in CTO, MTV, and APP/FTM. In APP/ATM, the throttle commands γ_{cmd} when ground speed is greater than 60 knots, and $\dot{h}_{cmd}$ when speed is less than 60 knots. In TRC, the throttle controls $\dot{h}_{cmd}$. At control mode switching, the new control sensitivity is bounded by an upper scaling slope and a lower scaling slope, figure 10, to prevent any unreasonable control sensitivity change due to the mode switch. This bounded envelope reflects a reasonable match between the physical throttle position and the thrust command, γ_{cmd}, and $\dot{h}_{cmd}$. To minimize any transient response during the throttle control's reconfiguration, the throttle control command is scaled to match the new control command state at the mode switch. Thus, if mode switching occurs within the bounded slopes at a steady flight condition, no transient response is introduced. The scaling logic is performed as follows:

At the mode switch, if the throttle position is greater than $(\delta_{th})_{ref}$, an upper throttle command scaling slope, $Slope_u$, is calculated based on the current throttle position, δ_{th}, and the maximum throttle travel, $(\delta_{th})_{max}$, the maximum command authority, $(\delta_{cmd})_{max}$, and the current state of the new throttle control parameter, δ, which is the thrust magnitude for the thrust command mode, flightpath angle for γ_{cmd} mode, or the vertical velocity for the $\dot{h}_{cmd}$ mode.

$$Slope_u = \frac{(\delta_{cmd})_{max} - \delta}{(\delta_{th})_{max} - \delta_{th}} \tag{4}$$

where δ_{cmd} is: T_{cmd} in CTO, MTV, and APP/FTM

γ_{cmd} in APP/ATM and $V_x \geq 60$ knots

$\dot{h}_{cmd}$ in $V_x < 60$ knots

This slope is bounded by the shaded area as shown in figure 10. The lower slope for $\delta_{th} < (\delta_{th})_{ref}$, $Slope_L$, is defined by equation 5 and 6.

$$(\delta_{cmd})_{ref} = (\delta_{cmd})_{max} - Slope_u \times [\,(\delta_{th})_{max} - (\delta_{th})_{ref}\,] \tag{5}$$

$$Slope_L = \frac{(\delta_{cmd})_{ref} - (\delta_{cmd})_{min}}{(\delta_{th})_{ref}} \tag{6}$$

The δ_{cmd} is then calculated as follows:

$$\begin{aligned} \delta_{cmd} &= (\delta_{cmd})_{ref} + Slope_u \times \left[(\delta_{th})_{max} - (\delta_{th})_{ref}\right] && \delta_{th} \geq (\delta_{th})_{ref} \\ \delta_{cmd} &= (\delta_{cmd})_{min} + Slope_L \times \delta_{th} && \delta_{th} < (\delta_{th})_{ref} \end{aligned} \tag{7}$$

The throttle controller is scaled from 0 to 100 percent travel, i.e., $(\delta_{th})_{max} = 100.0$, and the maximum and minimum δ_{cmd}, and the slopes are listed in table 5. The maximum and minimum slopes are selected to generate the reasonable mode switching transient response and logical throttle position for this experiment.

Thrust Management System

The flight control mode selected by the pilot determines the logic that allocates the core engine thrust to the nozzles and determines the engine nozzle deflection angles. The method used for the CTO mode, MTV mode, and the FTM portion of the APP mode will be presented first, followed by the method for the ATM portion of the APP mode and the TRC mode. The solutions for the propulsion effectors will satisfy either net thrust and thrust vector angle commands or vertical velocity and longitudinal acceleration commands. The control selector superimposes additional commands on those thrusts and deflections that the propulsion control system determines; these commands satisfy the pitch, roll and yaw SCAS, and will be discussed in detail in a later section of the paper. The response of the propulsion system to the final thrust commands will be discussed after the control selector.

In the CTO, MTV, and FTM portion of the APP mode, the pilot has direct control of the core engine thrust. In the CTO and MTV modes, the pilot directly controls the net thrust vector angle, while a longitudinal acceleration command/velocity hold loop commands this effector in the APP mode. With these control features in mind, the logic for determining the allocation of thrust to the cruise nozzle, lift nozzles and lift fan can be broken down into three basic cases once the lift fan is operative. The first propulsion system solutions that follow apply to those instances when the lift fan is inoperative, or when the commanded net thrust vector angle is less than or equal to zero deg, where the positive net thrust deflection angle is measured downward from the waterline of the aircraft. Figure 11 shows the convention for the nozzle deflection angles and the measurement of nozzle distances from the center of gravity. The net lift-fan thrust (T_{LF1}) and the net lift-nozzle thrust (T_{LN1}) are set equal to zero, and the longitudinal deflection angles of the lift fan and the lift nozzles are set to their maximum deflection values, that is, the deflection angle that directs the thrust of these nozzles as far aft as possible. The core engine thrust commanded by the pilot is $T_{T_{CMD}}$. The basic thrust equation for the aircraft, regardless of control mode, is:

$$\frac{T_{LF1}}{K_{AUG}\,\eta_{LF}} + \frac{T_{CN1}}{\eta_{CN}} + \frac{T_{LN1}}{\eta_{LN}} = T_{T_{CMD}} \tag{8}$$

In this equation, η_{LF}, η_{LN}, and η_{CN} are the efficiency factors of the lift fan, the lift nozzles and the cruise nozzle, respectively, and K_{AUG} is the lift-fan augmentation ratio. For the case in which the

pilot has manual control of the core engine thrust, the net cruise-nozzle thrust T_{CN1} is simply $T_{T_{CMD}}$ minus the core engine thrust that provides minimal lift-fan and lift-nozzle thrust, multiplied by η_{CN}. The cruise-nozzle deflection angle, δ_{CN}, is determined following the engine nozzle moment arm calculations. The lift-fan pitch moment arm and the lift-nozzle moment arm are calculated from the respective nozzle deflections, δ_{LF_x} and δ_{LN}, and the distances of these nozzles from the center of gravity of the aircraft:

$$L_{LF} = x_{LF} \cos \delta_{LF_x} + z_{LF} \sin \delta_{LF_x} \tag{9}$$

$$L_{LN} = -x_{LN} \cos \delta_{LN} - z_{LN} \sin \delta_{LN} \tag{10}$$

For this aircraft, equations 9 and 10 will always produce positive values for L_{LF} and L_{LN}. The cruise-nozzle deflection angle for which cruise-nozzle thrust does not produce a pitching moment on the aircraft, δ_{neu}, is calculated:

$$\delta_{neu} = -\tan^{-1}\left(\frac{z_{CN}}{x_{CN}}\right) \tag{11}$$

The distance from the cruise nozzle to the aircraft center of gravity (l_{CN}) is $\sqrt{(z_{CN})^2 + (x_{CN})^2}$. Longitudinal cruise-nozzle deflection is used to counteract the aerodynamic pitching moment, ΔM, as shown in equation 12:

$$\delta_{CN} = \sin^{-1}\left[\frac{-\Delta M - (T_{LF1})L_{LF} + (T_{LN1})L_{LN}}{(T_{CN1})l_{CN}}\right] + \delta_{neu} \tag{12}$$

where: $\Delta M = (C_{m_\alpha}\, \alpha + C_{m_{GE}}\, K_{GE} + C_{m_o})\, \bar{q} S \bar{c}$

C_{m_α} is the variation in pitching moment due to angle of attack

$C_{m_{GE}}$ is the variation in pitching moment due to ground effect

K_{GE} varies ground effect as a function of altitude

C_{m_o} is the pitching moment coefficient at zero angle of attack

The next case is applicable when the lift fan is engaged and the commanded net thrust vector angle is less than 45 deg. Table 6 shows the status of the propulsion system parameters for each group of solutions that follow for the MTV mode and the APP/FTM submode. As before, the lift-fan and lift-nozzle deflection angle are assumed to be at their maximum (aft) deflection, and the lift-nozzle thrust is set to zero. The propulsion system pitching moment equation can be written in terms of the nozzle thrusts and the vertical thrust component of the cruise nozzle, F_{CN_z}:

$$(T_{LF1})\,L_{LF} - (F_{CN_Z})\,x_{CN} = -\Delta M + (T_{LN1})\,L_{LN} \tag{13}$$

Using T_{CN1} as an approximation for the longitudinal component of the cruise-nozzle thrust, the net thrust deflection angle θ_N can be expressed in terms of the ratio of vertical thrust to longitudinal thrust:

$$\tan^{-1}\left(\frac{T_{LF1}\cos\delta_{LF_X} - F_{CN_Z}}{T_{LF1}\sin\delta_{LF_X} + T_{CN1}}\right) = \theta_N \tag{14}$$

Equation 14 can be rewritten as:

$$T_{LF1}[\cos\delta_{LF_X} - (\tan\theta_N)\sin\delta_{LF_X}] - T_{CN1}(\tan\theta_N) - F_{CN_Z} = 0 \tag{15}$$

As T_{LN1} is set to zero and $T_{T_{CMD}}$, θ_N, and δ_{LF_X} are known quantities, equations 13, 14, and 16 can be solved for T_{LF1}, T_{CN1} and F_{CN_Z}. F_{CN_Z} and T_{CN1} determine the cruise-nozzle deflection angle:

$$\delta_{CN} = \sin^{-1}\left(\frac{-F_{CN_Z}}{T_{CN1}}\right) \tag{16}$$

Equations 8, 13, 15, and 16 are used to determine T_{LF1}, T_{CN1}, and F_{CN_Z} until the cruise-nozzle deflection angle reaches its maximum (thrust directed downward) value. At this point, the lift-fan and lift-nozzle deflection angles are still set to their maximum value, and a different set of equations are used to determine the cruise-nozzle, lift-fan, and lift-nozzle thrusts. The thrust equation (eq. 8) is still applicable; none of the component thrusts are set to zero. With the cruise nozzle at its maximum deflection, the moment arm for the cruise nozzle is determined by:

$$L_{CN} = -x_{CN}\sin\delta_{CN} - z_{CN}\cos\delta_{CN} \tag{17}$$

The moment arms for the lift fan and the lift nozzles are determined with equations 9 and 10, with the nozzle deflection angles set to their maximum values. The pitching moment contributions of each nozzle appear in equation 18:

$$(T_{LF1})\,L_{LF} - (T_{LN1})\,L_{LN} + (T_{CN1})\,L_{CN} = -\Delta M \tag{18}$$

As in equation 15, the net thrust deflection angle can be expressed in terms of the nozzle thrusts. This equation incorporates the last known propulsion system parameter, the pilot's commanded value of θ_N:

$$\frac{T_{LF1}\cos\delta_{LF_X} + T_{CN1}\sin\delta_{CN} + T_{LN1}\cos\delta_{LN}}{T_{LF1}\sin\delta_{LF_X} + T_{CN1}\cos\delta_{CN} + T_{LN1}\sin\delta_{LN}} = \tan\theta_N \tag{19}$$

Equation 19 can be rewritten as:

$$T_{LF1}[\cos \delta_{LF_X} - \sin \delta_{LF_X} \tan \theta_N] + T_{LN1}[\cos \delta_{LN} - \sin \delta_{LN} \tan \theta_N]$$

$$+ T_{CN1}[\sin \delta_{CN} - \cos \delta_{CN} \tan \theta_N] = 0 \tag{20}$$

Equations 8, 18, and 20 can be solved for the three engine nozzle thrusts. If the lift-nozzle thrust or the lift-fan thrust resulting from these equations is below zero or above its maximum allowable value, then the equations for $T_{T_{CMD}}$ and pitching moment are solved again, with the lift-fan or lift-nozzle thrust set to the appropriate limit. If this solution exceeds another thrust limit, then the thrust allocation is determined with $T_{T_{CMD}}$ as the remaining constraint.

If the cruise-nozzle thrust calculated by equations 8, 18, and 20 is less than zero, or if the commanded net thrust deflection angle is greater than or equal to 45 deg, then the cruise-nozzle thrust is set to zero, and the cruise-nozzle deflection angle is set to its maximum (downward) value. This is the third propulsion control case for manual thrust control. The total thrust equation is essentially the same as equation 8, although T_{LF1} and T_{LN1} are the unknowns:

$$\frac{T_{LF1}}{K_{AUG}\,\eta_{LF}} + \frac{T_{LN1}}{\eta_{LN}} = T_{T_{CMD}} \tag{21}$$

The lift-fan and lift-nozzle deflection angles are equal and determined by the pilot's commanded thrust vector angle. Pitch moment arms are calculated for the lift fan and lift nozzle from equations 9 and 10. The relationship between the lift-fan thrust, the lift-nozzle thrust, and ΔM to balance the aircraft in pitch is:

$$(T_{LF1})\,L_{LF} - (T_{LN1})\,L_{LN} = -\Delta M \tag{22}$$

Equations 21 and 22 are solved simultaneously to find T_{LF1} and T_{LN1}. If the calculated T_{LF1} or T_{LN1} exceeds the nozzle limits, that thrust is limited accordingly and $T_{T_{CMD}}$ is used as the constraint in determining the thrust for other nozzle.

A different propulsion system control scheme is used for the APP/ATM submode and for the TRC mode. In these cases, the SCAS determines the forces (ΔX and ΔZ) and the pitching moment (ΔM) that the propulsion system must provide, and the propulsion system controller determines the appropriate nozzle deflection angles and nozzle thrusts.

The logic used in determining the propulsion system commands in the APP/ATM and TRC modes is similar to that used in the manual thrust modes. Once the lift fan is engaged, cruise-nozzle and lift-fan thrust alone are used for flightpath and speed control, with the fan nozzle set at its maximum (rearward) deflection angle. Once the cruise nozzle reaches its maximum (downward) deflection, lift-nozzle thrust is increased to satisfy the SCAS commands. The cruise-nozzle thrust is decreased as the vertical thrust needed for flightpath control increases, until all of the engine thrust is being directed to the lift fan and the lift nozzles. At this point, the lift fan and lift nozzles, which have been held at their aft deflection limits, are free to deflect as needed; the engine thrust is allo-

cated between these nozzles to satisfy powered lift and speed requirements in conjunction with the system's commanded nozzle deflection angles. This final propulsion system arrangement is used throughout the low-speed semi-jetborne flight regime (typically ≤ 120 knots IAS) and hover. Table 7 summarizes the thrust management solutions for these control modes.

For the first case with the lift fan engaged, the lift fan and lift nozzles are considered to be deflected fully aft, and the lift-nozzle thrust is set to zero. The vertical thrust equation is:

$$-T_{LF1} \cos \delta_{LF_X} + TGE_{LF} + F_{CN_Z} = \Delta Z \tag{23}$$

With the flightpath loop closed, the propulsion control system must compensate for thrust variations due to ground effects; the ground effect due to the lift-fan thrust is TGE_{LF}, and its value is determined from the actual lift-fan thrust that was commanded in the previous computer cycle. The thrust components that will provide the commanded longitudinal force, ΔX, are given by:

$$T_{LF1} \sin \delta_{LF_X} + F_{CN_X} = \Delta X \tag{24}$$

The moment arms of the lift fan and the lift nozzles are determined by equations 9 and 10, the same method that was used in the manual thrust cases. With the pitching moment increment due to ground effect represented as MGE_{LF}, the thrust contribution to pitching moment is:

$$T_{LF1} L_{LF} + MGE_{LF} - (F_{CN_Z})x_{CN} + (F_{CN_X})z_{CN} = -\Delta M \tag{25}$$

Using the SCAS values for desired longitudinal force, vertical force, and pitching moment, equations 23–25 are solved simultaneously for T_{LF1}, F_{CN_X} and F_{CN_Z}. The vector sum of F_{CN_X} and F_{CN_Z} determines the net cruise-nozzle thrust, T_{CN1}, and the ratio of F_{CN_Z} to T_{CN1} determines the deflection angle of the cruise nozzle. If the lift-fan thrust calculated in this manner exceeds the maximum allowable lift-fan thrust, the fan thrust is set to that maximum and F_{CN_Z} is recalculated to provide the pitching moment for aircraft trim.

Once the aircraft has slowed to the point that a significant portion of the lift-fan thrust is required to maintain the commanded flightpath angle, the cruise nozzle reaches its maximum downward deflection angle because the pitch trim of the aircraft must be maintained. Once this occurs, the cruise-nozzle deflection is fixed at its maximum value and a different set of equations is used to determine the lift-fan, lift-nozzle and cruise-nozzle thrust. The lift fan and lift nozzle are still deflected fully aft. The vertical, longitudinal and pitching moment thrust equations that determine T_{LF1}, T_{CN1} and T_{LN1} are:

$$-T_{LF1} \cos \delta_{LF_X} + TGE_{LF} - T_{LN1} \cos \delta_{LN} + TGE_{LN} - T_{CN1} \sin \delta_{CN} = \Delta Z \tag{26}$$

$$T_{LF1} \sin \delta_{LF_X} + T_{LN1} \sin \delta_{LN} + T_{CN1} \cos \delta_{CN} = \Delta X \tag{27}$$

$$T_{LF1} L_{LF} + MGE_{LF} - T_{LN1} L_{LN} + MGE_{LN} + (T_{CN1})L_{CN} = -\Delta M \tag{28}$$

If one of the solutions to these three equations violates a thrust limit, then that nozzle's thrust is set to its limit and the ΔX and ΔM equations are solved to find the remaining nozzle thrusts. If a second thrust limit is encountered, the last thrust value is determined with the moment equation and the other thrusts set to the appropriate limits. In this way, as propulsion limits are reached, the control of the vertical axis is given up first, followed by control of the longitudinal axis. This axis priority prevents thrust commands that could send the aircraft into a violent pitch excursion.

Equations 26–28 are used for thrust allocation until the cruise-nozzle thrust solution is less than or equal to zero. At this point, new solutions involving not only nozzle thrusts but also lift-fan and lift-nozzle deflection angles are used. In the original design of the propulsion system, the longitudinal lift-fan deflection limit and the lift-nozzle deflection limits were not the same, and therefore it could not be assumed that these nozzles would ever be at the same deflection angle. To solve for the four unknowns with the two forces and one moment that the SCAS requires, the ratio of ΔX to ΔZ was used to determine the deflection angle of the lift fan. The longitudinal deflection angle of the lift fan is expressed as:

$$\delta_{LF_x} = \tan^{-1}\left(\frac{\Delta X}{-\Delta Z}\right) \tag{29}$$

The lift-nozzle deflection angle, the lift-fan thrust and the lift-nozzle thrust are found by simultaneous solution of the following vertical, longitudinal and pitching moment thrust equations:

$$-T_{LF1} \cos \delta_{LF_x} + TGE_{LF} + F_{LN_z} + TGE_{LN} = \Delta Z \tag{30}$$

$$T_{LF1} \sin \delta_{LF_x} + F_{LN_x} = \Delta X \tag{31}$$

$$T_{LF1}\, L_{LF} + MGE_{LF} - (F_{LN_Z})\, x_{LN} + MGE_{LN} + (F_{LN_x}) z_{LN} = -\Delta M \tag{32}$$

The lift-nozzle thrust and deflection angle are determined by the thrust vector components F_{LN_x} and F_{LN_z}. As in the case of equations 26–28, control over the longitudinal axis is relinquished first, followed by control over the vertical axis, as nozzle deflection limits and nozzle thrust limits are reached. This change in axis control priority reflects the low-speed flight conditions for which equations 30–32 are used, as the engine must provide most or all of the aircraft's lift.

Control Selector

A diagram of the control selector appears in figure 12. The control selector combines preliminary propulsion system and aircraft attitude commands to generate control surface deflections, final propulsion system nozzle deflections, reaction control system deflections, and final propulsion system thrust commands. As the response of the control surface and engine nozzle actuators was considered to be fast, the computational delay of the computer provided an adequate lag to duplicate the response of these components. No explicit model of these actuators was created or used.

Commands from the pitch SCAS drive the canard directly. The canard deflection limits are 30 deg trailing edge up and 10 deg trailing edge down. When the lift fan is in use, pitch commands are multiplied by the gain KLF and added to the lift-fan thrust from the propulsion controller, T_{LF1}, to produce the final lift-fan thrust command. The value of KLF depends upon the current lift-fan thrust and the total core thrust, T_{TOT}. If the core thrust currently diverted to the lift fan exceeds the core engine thrust diverted to the remaining engine nozzles, then:

$$KLF = \frac{1}{30}\left(T_{TOT} - \frac{T_{LF}}{\eta_{LF} K_{AUG}}\right) \tag{33}$$

Otherwise, KLF is set to 1/30 of the core thrust that is currently being used to drive the lift fan. The maximum lift-fan thrust is 17,400 lb KPLN, which is used to modify the thrust of each lift nozzle, is set equal to half of KLF; thus, pitch commands transfer the same amount of core engine thrust between the lift nozzles and the lift fan. If the pitch RCS option has been selected, the switch IRCSP is set equal to one and the pitch commands, multiplied by KPRCS (41.67 lb/deg of canard deflection), cause deflection of the pitch reaction control nozzles; the maximum pitch RCS thrust is 1,250 lb, directed either upward or downward depending on the sign of the pitch command.

Roll control is generated by the ailerons in wingborne flight and through thrust transfer between the lift nozzles in jetborne flight, scaled per degree of aileron deflection. The deflection limits for the ailerons are ±30 deg. After taking into account lift-fan/lift-nozzle thrust transfer due to pitch commands, the amount of thrust to be transferred differentially between the lift nozzles is determined. KRLN is determined by the current value of lift-nozzle thrust and T_{TOT}. If the thrust of both lift nozzles exceeds the remaining core engine thrust, then:

$$KRLN = \frac{1}{60}(T_{TOT} - T_{LN}) \tag{34}$$

If the combined lift-nozzle thrust is less than the core engine thrust, then KRLN is set to 1/60 of T_{LN}. The roll commands are summed with the lift-nozzle thrust determined by the propulsion control system to produce the right and left lift-nozzle thrust commands. Each lift-nozzle thrust is limited to 12,000 lb. When the lift-nozzle deflection angle does not coincide with the vertical axis of the aircraft, differential lift-nozzle thrust produces uncommanded yawing moments on the aircraft. To counteract these moments, the system uses lateral deflection of the lift-fan nozzle. The interconnect gain between differential lift-nozzle thrust and lateral lift-fan nozzle deflection is KRY1, which is determined by:

$$KRY1 = \left(\frac{y_{LN}}{x_{LF}}\right)\sin(\delta_{LN}) \tag{35}$$

A yaw RCS can be used instead of the lift-fan nozzle to produce yawing moments. If this option is selected, then KRY1 is multiplied by (x_{LF} / x_{RCS}). Usually the roll RCS is not employed; however, when IRCSR is set equal to 1 to enable this system, the gain KRRCS is set equal to 83.33 lb/deg, with reaction control thrust limit of 2500 lb.

Rudder deflection, differential lift-nozzle deflection, and lateral lift-fan deflection all provide yaw control for the aircraft. Commands from the yaw SCAS directly drive the rudder, which is limited to ±30 deg of deflection. Five deg of differential lift-nozzle deflection are available for yaw axis control in the powered lift regime. It follows that KYLN is 1/30 of 5 deg; the product of the yaw command and KYLN is added to the lift-nozzle deflection determined by the propulsion control system to produce the final left and right lift-nozzle deflection angles. The yaw command also produces lateral lift-fan deflection in the powered lift regime. KYLF is set to the same value as KYLN, and after KYLF is multiplied by the yaw command, the differential lift-nozzle thrust interconnect signal is added to it, resulting in the lateral deflection command for the lift-fan nozzle. The deflection of this nozzle is limited to ±15 deg, positive deflection producing positive side force. If the IRCSY flag is set to one, the yaw RCS is used instead of lateral lift-fan nozzle deflection. KYRCS is set to 41.67 lb of RCS thrust per degree of yaw command. After the differential lift-nozzle thrust interconnect is added to this signal, the yaw RCS command is limited to ±1,250 lb.

Propulsion System

The propulsion system model developed for this experiment is a representation of a lift fan coupled to a lift/cruise engine as shown in figure 2. The 2-dimensional convergent-divergent (2D-CD) nozzle of the lift/cruise engine provides axial thrust in cruise and vectoring thrust during transition. Thrust can be transferred from the 2D-CD nozzle to a pair of lift nozzles and to the lift fan to produce longitudinal and vertical thrust during transition and hover.

The lift/cruise engine responds to total thrust command, $T_{T_{CMD}}$, which is calculated as a sum of the individual nozzle thrust commands that are generated from the control selector. The closed loop core thrust dynamic response is model by a second order transfer function with respect to a referenced core engine state, $T_{T_{Ref}}$. $T_{T_{Ref}}$ is defined as the trim state of the core thrust response and is reset to the total thrust response, T_{TOT}, whenever the engine reaches a steady state. An incremen tal thrust command, $\Delta T_{T_{CMD}}$, is calculated from the total thrust command and the referenced thrust as shown in equation 37. This incremental thrust command is then fed through a second order transfer function which represents the closed-loop core engine dynamic characteristics, where the damping ratio is set to 0.707 and the bandwidth, ω_{core}. A rate limit, $\dot{T}_{T_{max}}$, and a lift/cruise engine thrust magnitude limit, $T_{T_{max}}$, are included in the second order transfer function model to represent physical thermal limits of the propulsion system. Each individual nozzle's referenced thrust and the response due to perturbed lift/cruise engine are distributed proportionally by the ratio of each nozzle thrust command over the total thrust command, equations 41 and 42.

$$T_{T_{CMD}} = T_{CN_{CMD}} + T_{LLN_{CMD}} + T_{RLN_{CMD}} + T_{LF_{CMD}} / K_{AUG} \tag{36}$$

where K_{AUG} is the lift-fan augmentation ratio

$$\Delta T_{T_{CMD}} = T_{T_{CMD}} - T_{T_{Ref}} \tag{37}$$

$$\Delta T_T = \left(\frac{\omega_{core}^2}{s^2 + 2\zeta\omega_{core}s + \omega_{core}^2} \right) \Delta T_{T_{CMD}} \tag{38}$$

$$T_{TOT} = T_{T_{Ref}} + \Delta T_T \tag{39}$$

$$R_i = \frac{T_{i_{CMD}}}{T_{T_{CMD}}} \tag{40}$$

where i = CN, LLN, RLN, and LF

$$T_{i_{Ref}} = T_{T_{Ref}} R_i \tag{41}$$

$$\Delta T_{i\ CORE} = \Delta T_T R_i \tag{42}$$

To model the thrust transfer rate limit effect, the thrust transfer command for each nozzle is defined as,

$$\Delta T_{i_{TF}} = T_{i_{CMD}} - T_{i_{Ref}} - \Delta T_{T_{CMD}} R_i \tag{43}$$

The thrust transfer rate for each nozzle, $\dot{T}_{i_{TF}}$, is limited to $\dot{T}_{TF_{max}}$.

The thrust response for each nozzle is calculated as shown in equation 44, in which η is the thrust recovery factor for each specified nozzle.

$$T_{CN} = (T_{CN_{Ref}} + \Delta T_{CN_{CORE}} + \Delta T_{CN_{TF}}) \times \eta_{CN} \tag{44}$$

$$T_{LLN} = (T_{LLN_{Ref}} + \Delta T_{LLN_{CORE}} + \Delta T_{LLN_{TF}}) \times \eta_{LN}$$

$$T_{RLN} = (T_{RLN_{Ref}} + \Delta T_{RLN_{CORE}} + \Delta T_{RLN_{TF}}) \times \eta_{LN}$$

$$T_{LF0} = T_{LF_{Ref}} + \Delta T_{LF_{CORE}} + \Delta T_{LF_{TF}}$$

For this experiment, a generic energy transfer between the lift/cruise engine and the lift fan is assumed. Dynamically, the lift-fan thrust at the lift-fan nozzle exit, T_{LF}, due to T_{LF0} from equation 44 is dependent on lift-fan rotational speed and inlet guide vane setting. The dynamic response is modeled by a first order transfer function with a time constant of ω_{LF}, plus a first order washout transfer function, as shown in figure 13 . A rate limit, $\dot{T}_{LFmax}$, and a maximum lift-fan thrust limit, T_{LFmax}, are included to represent physical constraints of the lift-fan dynamics. The upper and lower IGV authorities are defined as shown in equation 45, in which K_{IGV_U} and K_{IGV_L} are in percent of lift-fan inertia thrust.

$$TIGV_U = K_{IGV_U} T_{LF_S}, \quad TIGV_L = K_{IGV_L} T_{LF_S} \tag{45}$$

The total lift-fan thrust, T_{LF}, is then calculated from the fan inertia thrust and IGV thrust as shown in equation 46, where η_{LF} is a generic thermal/mechanical efficiency constant.

$$T_{LF} = (T_{LF_S} + T_{LF_F}) \times \eta_{LF} \tag{46}$$

The mass flow rates of the primary inlets and auxiliary inlets are functions of the total thrust, maximum lift/cruise engine thrust, and respective maximum mass flow rate as shown in equations 47 and 48. A maximum mass flow rate of 11.2 slug/sec was used in each case. Primary inlets are opened in CTO and APP, and are closed in TRC. Auxiliary inlets are only opened in TRC to reduce the amount of hot gas reingestion. The mass flow rate of the lift-fan inlet is modeled as a function of the lift-fan thrust, maximum lift-fan thrust, and the maximum lift-fan mass flow rate (eq. 49) which was set to 14.0 slug/sec.

$$\dot{m}_{PI} = \left(\frac{T_{TOT}}{T_{TMAX}} \right) \dot{m}_{P\,Imax} \tag{47}$$

$$\dot{m}_{AI} = \left(\frac{T_{TOT}}{T_{TMAX}} \right) \dot{m}_{A\,Imax} \tag{48}$$

$$\dot{m}_{LFI} = \left(\frac{T_{LF}}{T_{LFMAX}} \right) \dot{m}_{LF\,Imax} \tag{49}$$

The resulting propulsion forces and moments are resolved into the aircraft body axes from each individual nozzle thrust and deflection, inlets, and reaction control system (RCS) when it is activated.

Axial force:

$$F_{EX} = F_{CN_X} + F_{LLN_X} + F_{RLN_X} + F_{LF_X} + F_{PI_X} + F_{AI_X} + F_{LFI_X} \tag{50}$$

where $F_{CN_X} = T_{CN} \cos \delta_{CN}$

$F_{LLN_X} = T_{LLN} \sin \delta_{LN}$

$F_{RLN_X} = T_{RLN} \sin \delta_{LN}$

$F_{LF_X} = T_{LF} \sin \delta_{LF_X} \cos \delta_{LF_y}$

$F_{PI_X} = -\dot{m}_{PI} U_B$

$F_{AI_X} = -\dot{m}_{AI} U_B$

$F_{LFI_X} = \dot{m}_{LFI} (-U_B - Q_B z_{PI})$

Side force:

$$F_{EY} = F_{LF_y} + F_{PI_y} + F_{AI_y} + F_{LFI_y} + F_{RCS_y} \tag{51}$$

where $F_{LF_y} = T_{LF} \sin \delta_{LF_y}$

$F_{PI_X} = \dot{m}_{PI} (-V_B + P_B z_{PI} - R_B x_{PI})$

$F_{AI_X} = \dot{m}_{AI} (-V_B + P_B z_{AI} - R_B x_{AI})$

$F_{LFI_X} = \dot{m}_{LFI} (-V_B + P_B z_{LFI} - R_B x_{LFI})$

Normal force:

$$F_{EZ} = F_{CN_Z} + F_{LLN_Z} + F_{RLN_Z} + F_{LF_Z} + F_{PI_Z} + F_{AI_Z} + F_{LFI_Z} \tag{52}$$

where $F_{CN_Z} = T_{CN} \sin \delta_{CN}$

$F_{LLN_Z} = T_{LLN} \cos \delta_{LN}$

$F_{RLN_Z} = T_{RLN} \cos \delta_{LN}$

$F_{LF_Z} = T_{LF} \cos \delta_{LF} \cos \delta_{LF_y}$

$F_{PI_Z} = -\dot{m}_{PI} W_B$

$F_{AI_Z} = -\dot{m}_{AI} W_B$

$F_{LFI_Z} = \dot{m}_{LFI} (-W_B + Q_B x_{PI})$

Rolling moment:

$$T_{EL} = -F_{LLN_Z} y_{LLN} + F_{RLN_Z} y_{RLN} + F_{LFY_Z} z_{LF} \quad (53)$$
$$+ F_{RCSY_Z} z_{RCS} + F_{RCS_y} z_{RCS} F_{RCS_Z} y_{RCS}$$
$$- F_{PI_y} z_{PI} - F_{AI_y} z_{AI} - F_{LFI_y} z_{LFI}$$

Pitching moment:

$$T_{EM} = -F_{CN_Z} x_{CN} - F_{LLN_Z} x_{LLN} + F_{RLN_Z} x_{RLN} - F_{LF_Z} x_{LF} \quad (54)$$
$$+ F_{CN_X} z_{CN} + F_{LLN_X} z_{LLN} + F_{RLN_X} z_{RLN} - F_{LF_X} z_{LF}$$
$$- F_{PI_Z} x_{PI} - F_{AI_Z} x_{AI} - F_{LFI_Z} x_{LFI}$$
$$+ F_{PI_X} z_{PI} - F_{AI_X} z_{AI} - F_{LFI_X} z_{LFI}$$

Yawing moment:

$$T_{EN} = F_{LLN_X} y_{LLN} - F_{RLN_X} y_{RLN} + F_{LFY_Z} z_{LF} \quad (55)$$
$$+ F_{RCSY_Z} x_{RCS} + F_{LF_y} x_{LF}$$
$$+ F_{PI_y} x_{PI} + F_{AI_y} x_{AI} + F_{LFI_y} x_{LFI}$$

Head Up Display

A head-up display (HUD), that has been employed by NASA in several previous V/STOL simulations, provided the primary flight display for this experiment. The display is described here in general terms. The reader should consult reference 7 for a complete description of symbology and drive laws.

Separate presentations were adopted for transition and hover. For the transition phase, shown in detail in figure 14, the display was a flightpath centered, pursuit presentation that enhanced the external visual cues, centered them on the aircraft's flightpath, and presented the pilot with a pursuit tracking task for following the intended transition and approach guidance to a final hover point. Course and glideslope guidance was provided in the form of a lead (ghost) aircraft that followed the desired flight profile. The pilot's task was to track the ghost aircraft with the flightpath symbol. As indicated in reference 7, the flightpath symbol was quickened to compensate for lags in the airframe and propulsion system response. For the MTV or FTM control modes, where thrust was controlled manually using the throttle, the flightpath compensation included lagged pitch rate and washed out throttle commands in combination with the true flightpath in accord with the following equation:

$$\gamma_q = \frac{K_{q\dot{\theta}}}{s+\sigma_w} + \tan^{-1}\left(\frac{K_{\delta_T}\delta_T}{V_T}\right)\left(\frac{s}{s+\sigma_w}\right) + \tan^{-1}\left(\dot{h}/V_T\right) \tag{56}$$

and $\sigma_w = Z_{w_{hover}} + V_{af}\, Z'_w$ $\qquad Z_{w_{hover}} = g(\dot{m}_e/W)$

$Z'_w = 1.58\ \rho g S/W$ $\qquad K_{\delta_T} = A_{\delta_T} \sin\theta_j / \sigma_w$

The pitch rate term was blended out for speeds below 55 knots and true airspeed was frozen at 100 ft/sec for speeds less than 100 ft/sec. Gains and washout frequencies were $K_q = 1$, $A_{\delta_T} = 0.3$. For ATM, the flightpath was complemented with its commanded value in the short term according to

$$\gamma_q = \tan^{-1}\frac{\dot{h}_c}{V_T}\left(\frac{s}{s+\omega_\gamma}\right) + \tan^{-1}\left(\dot{h}/V_T\right) \tag{57}$$

The washout frequency ω_γ was 1 rad/sec. True lateral flightpath was represented by the flightpath symbol. Deceleration guidance was presented by an acceleration error ribbon on the right side of the flightpath symbol which the pilot nulled to follow the deceleration schedule. Situation information that accompanied the flightpath and ghost aircraft symbology included aircraft attitude, speed, altitude, engine rpm, thrust vector angle, longitudinal acceleration, heading, and distance to the hover point.

During the latter stages of the deceleration as the aircraft approaches the intended point of hover, selective changes are made to the approach display to provide guidance for the hover point capture. Specifically, the longitudinal velocity vector, predicted longitudinal velocity, and station keeping cross appear referenced to the vertical velocity diamond symbol as shown in figure 15. The drive law for predicted longitudinal velocity is shown below in the discussion of the hover display (eq. 58). The pilot controls the predicted velocity toward the station keeping cross position and adjusts velocity to bring the cross to rest at the reference hover point indicated by the cross being adjacent to the vertical velocity diamond. Once the aircraft is stabilized in this condition, the pilot is ready to perform the vertical landing.

For the vertical landing, including recovery to the ship, the HUD format superimposed vertical and plan views and provided command and situation information in a pursuit tracking presentation (fig. 16). In the horizontal situation, the aircraft velocity vector was represented by a line emanating from the aircraft symbol. A pad symbol represented the landing area. Horizontal and vertical velocity predictor symbols, whose displacement and orientation from the aircraft symbol indicated magnitude and direction provided the pilot lead information for hover maneuvering. Predicted horizontal and vertical velocity presentations were compensated for aircraft and propulsion system lags as they were for transition. In this case, for MTV mode, true velocities were complemented with translational accelerations and washed out control commands according to the relationship:

$$V_{x_c} = V_x + \frac{T\dot{v}}{s+1/T_6}\left[\dot{V}_x - g\left(\dot{\theta}+\dot{\theta}_j\right)\left(\frac{s}{s+\sigma_u}\right)\right] - K_{\theta_c}\theta_c\left(\frac{s}{s+1/T_2}\right) \tag{58}$$

where $\sigma_u = X_{u_{hover}} + V_{af}\, X'_u \qquad X_{u_{hover}} = g(\dot{m}_e/W) \qquad X'_u = C_{D_{aero}}\, \rho g S/W$

$T_{\dot{v}} = 1.11 \qquad T_6 = 10 \qquad K_{\theta_c} = 3.45 \qquad T_2 = 10$

For TRC mode, the commanded horizontal velocities were displayed directly. The vertical situation was displayed by a diamond referenced to the left leg of the aircraft symbol whose displacement, t_{w_c}, was proportional to complemented vertical speed. For MTV mode vertical velocity is complemented with vertical acceleration so that

$$t_{w_c} = K_w\left[\dot{h} + \frac{T_{\dot{h}}}{T_6 s+1}\left(\ddot{h} + K_{\delta_T}\delta_T T_6 \frac{s^2}{s+\sigma_w}\right)\right] \tag{59}$$

where $K_w = 0.2$ and the other terms have the same values as for the flightpath symbol drive. When TRC is engaged vertical velocity was complemented with washed out vertical velocity command to provide the command

$$t_{w_c} = K_w\left[\dot{h} + \dot{h}_c\left(\frac{s}{s+\omega_\gamma}\right)\right] \tag{60}$$

and $\omega_\gamma = 1$. A horizontal bar indicated the altitude remaining to touchdown. Attitude, air velocity, engine rpm, thrust vector angle, heading, vertical velocity limits, and wind direction are provided as situation information.

CONCLUSIONS

A simulation model of an integrated flight/propulsion control system, propulsion system, and head-up display has been developed for an advanced, short takeoff, vertical landing lift-fan fighter aircraft. These models, combined with a model of the aircraft' s aerodynamic characteristics have been employed in piloted evaluations of takeoff, transition, hover, and landing characteristics of this class of aircraft. The flight/propulsion control system includes modes for several response types which are coupled to the aircraft's aerodynamic and propulsion system effectors through a control selector tailored to the lift-fan propulsion system. Design of the system has drawn on experience gained from simulation of earlier STOVL configurations, including the Mixed Flow Vectored Thrust and Augmentor Ejector concepts as well as from the VSTOL Systems Research Aircraft, which is a modification of the YAV-8B Harrier prototype. Propulsion system components modeled include a remote lift-fan and a lift/cruise engine. Their static performance and dynamic response are represented by the model. A separate report describes the subsonic, power-off aerodynamics and jet induced aerodynamics in hover and forward flight, including ground effects.

REFERENCES

1. Engelland, S. A.; Franklin, J. A.; and McNeill, W. E.: Simulation Model of a Mixed-Flow Remote-Lift STOVL Aircraft. NASA TM-102262, Feb. 1990.

2. Birckelbaw, L. G.; McNeill, W. E.; and Wardwell, D. A.: Aerodynamics Model for a Generic ASTOVL Lift-Fan Aircraft. NASA TM-110347, Apr. 1995.

3. Franklin, J. A.; Hynes, C. S.; Hardy, G. H.; Martin, J. L.; and Innis, R. C.: Flight Evaluation of Augmented Controls for Approach and Landing of Powered-Lift Aircraft. AIAA Journal of Guidance, Control, and Dynamics, vol. 9, no. 5, Sept.–Oct. 1986.

4. Franklin, J. A.; Stortz, M. W.; Gerdes, R. M.; Hardy, G. H.; Martin, J. L.; and Engelland, S. A.: Simulation Evaluation of Transition and Hover Flying Qualities of the E-7A STOVL Aircraft. NASA TM-101015, Aug. 1988.

5. Franklin, J. A.; Stortz, M. W.; Engelland, S. A.; Hardy, G. H.; and Martin, J. L.: Moving Base Simulation of Control System Concepts and Design Criteria for STOVL Aircraft. NASA TM-103843, June 1991.

6. Chung, W. W.; McNeill, W. E.; and Stortz, M. W.: A Direct Application of the Non-Linear Inverse Transformation Flight Control System Design on a STOVL Aircraft. NASA TM-108808, May 1993.

7. Merrick, V. K.; Farris, G. G.; and Vanags, A. A.: A Head Up Display for Application to V/STOL Aircraft Approach and Landing. NASA TM-102216, Jan. 1990.

Table 1. Aircraft geometry

	Overall length	55.4 ft
	Overall height	14.16 ft
Wing	Area	523.3 ft^2
	Span	36.17 ft
	Mean aerodynamic chord	18.42 ft
	Aspect ratio	2.50
	Leading edge sweep	40.0 deg
	Trailing edge sweep	30.0 deg
	Airfoil	NACA 64A005
Canard	Area	243.1 ft^2
	Span	24.65 ft
	Mean aerodynamic chord	12.55 ft
	Aspect ratio	2.50
	Leading edge sweep	40.0 deg
	Trailing edge sweep	30.0 deg
	Airfoil	NACA 64A004.5
Vertical tail (each)	Area	39.0 ft^2
	Span	6.98 ft
	Mean aerodynamic chord	7.11 ft
	Aspect ratio	1.25
	Leading edge sweep	40.0 deg
	Trailing edge sweep	30.0 deg
	Airfoil	NACA 64A004.5

Table 2. Mass properties

Weight	30,000 lb
x cg location	373.3 in.
y cg location	0.0 in.
z cg location	96.0 in.
Pitch moment of inertia	91,200 slug-ft^2
Roll moment of inertia	14,300 slug-ft^2
Yaw moment of inertia	101,000 slug-ft^2
Product of inertia	0 slug-ft^2

Table 3. Flight control modes

Control axis	Control mode designations (applicable flight phases)			
	CTO (wingborne flight)	MTV (transition, hover) APP: FTM (transition)	APP: ATM (transition, hover)	TRC (hover)
Pitch/roll	Rate command - attitude hold	Rate command - attitude hold, blend to attitude command	Rate command - attitude hold, blend to attitude command	
Yaw	Sideslip command	Sideslip command, blend to yaw rate command	Sideslip command, blend to yaw rate command	Yaw rate command
Vertical	Aerodynamic lift	Thrust magnitude	Flightpath command, blend to velocity command	Velocity command
Longitudinal	Thrust magnitude	Thrust vector angle (MTV), acceleration command - velocity hold (APP)	Acceleration command - velocity hold	Velocity command
Lateral				Velocity command

Table 4. Control mode gains

Attitude control	
Pitch	Roll
Control limits = ±5.65 in.	Control limits = ±4.2 in.
Force gradient = 1.0 lb/in.	Force gradient = 0.7 lb/in.
Breakout = 0.15 in.	Breakout = 0.05 in.
K_{111} = 0.28 rad/sec/in.	K_1 = 1.2 rad/in.
K_{222} = 0.3 rad/in.	K_{333} = 1.6 rad/sec/in.
K_θ = 4.0 rad/rad	K_ϕ = 9.0 rad/rad
$K_{\dot{\theta}}$ = 4.0 sec	$K_{\dot{\phi}}$ = 6.0 sec
$K_{300} = 20.0/(1 + 0.0047\bar{q})$ deg/rad	$K_3 = 15.0\ (100/KRLN)/(1 + 0.029\bar{q})$ deg/rad
τ_9 = 0.05 sec	τ_8 = 0.05 sec
Yaw - transition	Yaw - Hover
Control limits = ±2.12 in.	Same
Force gradient = 14.0 lb/in.	Same
Breakout = 0.1 in.	Same
K_{10} = 0.3 rad/in.	K_{10H} = 2.3
$K_{\dot{\beta}}$ = 2.8 sec	$K_{\dot{\psi}}$ = 4.0 sec
K_β = 40 rad/rad	K_{30} = 40.0 deg/rad
τ_β = 0.25 sec	K_B = 0 (V ≤ 40 knots); 1.0 (V ≥ 50 knots)
	τ_7 = 0.05 sec
Velocity control	
Longitudinal velocity	Vertical velocity
Control limits	K_γ = 0.00545 rad/deg
Stick = ±2.25 in.	$K_w = 0.71\ sec^{-1}$
Thumbwheel = ±100 deg	K_{3W} = 0.14
Breakout	τ_{CNT} = 0.1 sec
Stick = 0.225 in.	
Thumbwheel = 5.5 deg	Lateral velocity
$K_{2\dot{U}}$ = 0.1	K_6 = 10.0 ft/sec/deg
$K_{VI} = 20.0\ sec^{-1}$	PR = 5.25
$K_V = 14.0\ ft/sec^2/in.$	$K_{\phi 2}$ = 0.58 rad/ft/sec
$K_U = 0.69\ sec^{-1}$	K_9 = 0.285 rad/rad
K_{3U} = 1.0	
τ_U = 0.35 sec	

Table 5. Maximum and minimum throttle control commands and control sensitivity slopes

δ_{cmd}	Maximum	Minimum	Max slope$_u$ ($1/\delta_{th}$) 1/%	Min slope$_u$ ($1/\delta_{th}$) 1/%
Thrust magnitude, %	100	3	1.0	0.5
Flightpath angle, γ, deg	10	–20	0.3	0.287
Vertical velocity, $\dot{h}$, ft/sec	20	–40	0.6	0.5

Table 6. Propulsion management summary for MTV and APP:FTM modes

Case	T_{CN1}	δ_{CN}	T_{LF1}	δ_{LF_X} ($=\delta_{LN}$)	T_{LN1}	Equations in text
1. Lift fan engaged and θ_N < 45 deg	Unknown	Unknown	Unknown	Maximum	0	8, 13, 15, 16
2. Case 1 $\delta_{CN} \geq$ max.	Unknown	Maximum	Unknown	Maximum	Unknown	8, 18, 20
3. Case 2 $T_{CN1} \leq$ 0 or θ_N > 45 deg	0	Maximum	Unknown	θ_N	Unknown	21, 22

Table 7. Propulsion management summary for APP:ATM and TRC modes

Case	T_{CN1}	δ_{CN}	T_{LF1}	δ_{LF_X}	T_{LN1}	δ_{LN}	Equations in text
1. Lift fan engaged	Unknown	Unknown	Unknown	Maximum	0	Maximum	23, 24, 25
2. Case 1 $\delta_{CN} \geq$ max.	Unknown	Maximum	Unknown	Maximum	Unknown	Maximum	26, 27, 28
3. Case 2 $T_{CN1} \leq$ 0	0	Maximum	Unknown	Unknown	Unknown	Unknown	29, 30, 31, 32

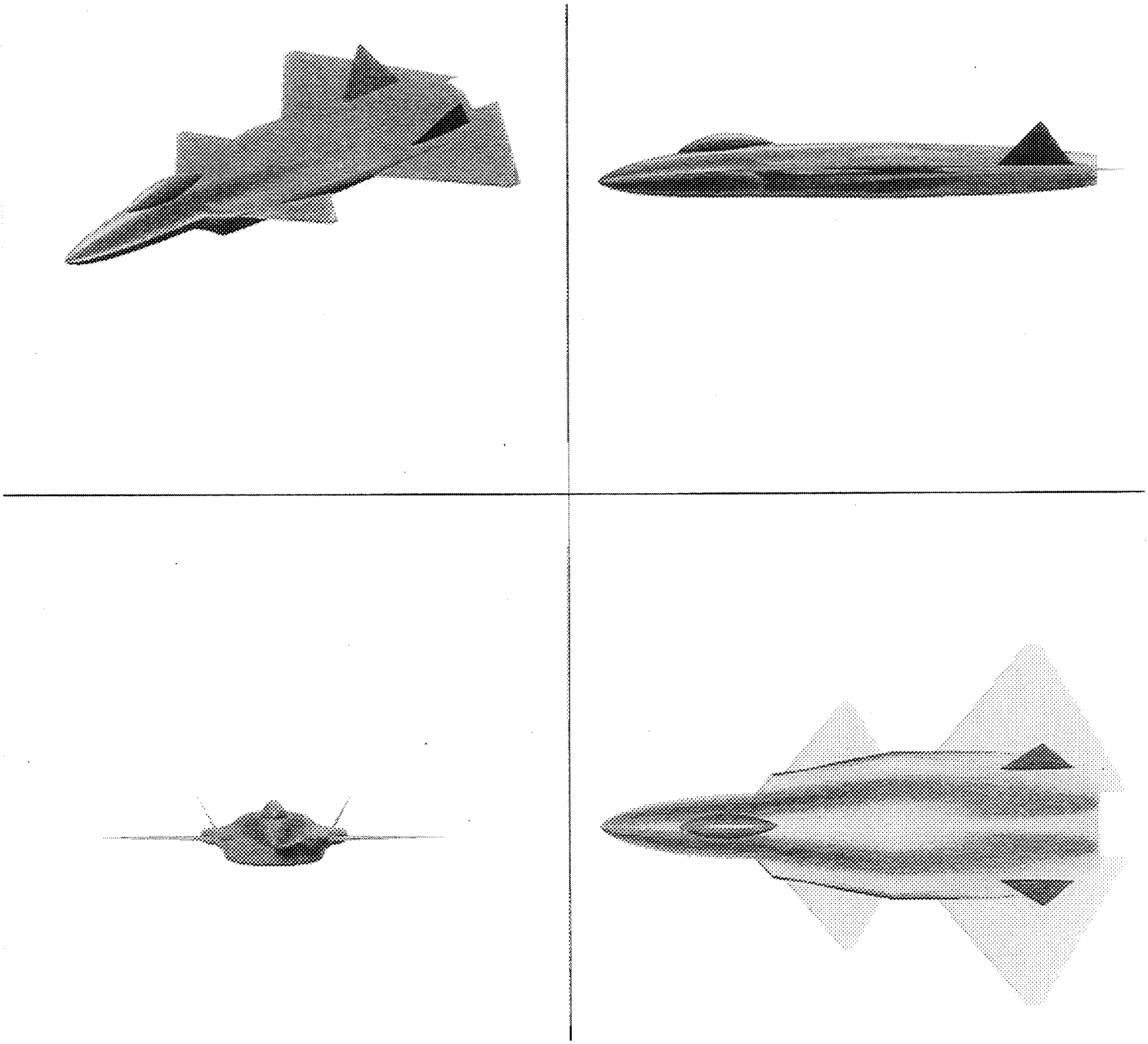

Figure 1. Views of the ASTOVL Lift Fan Aircraft.

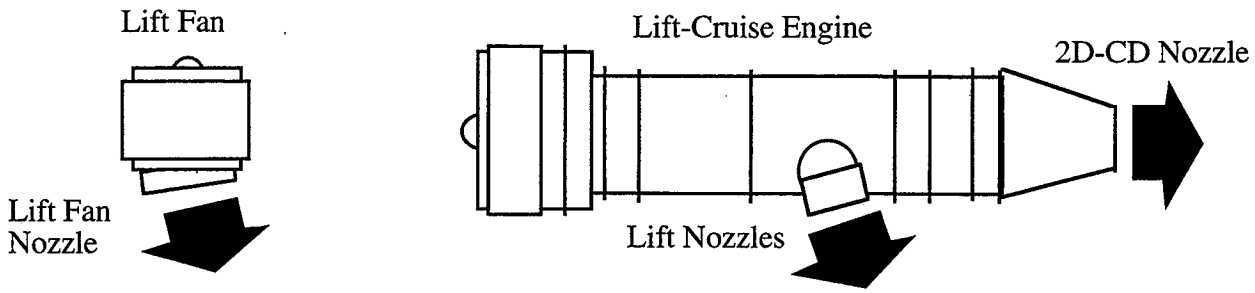

Figure 2. Propulsion system configuration.

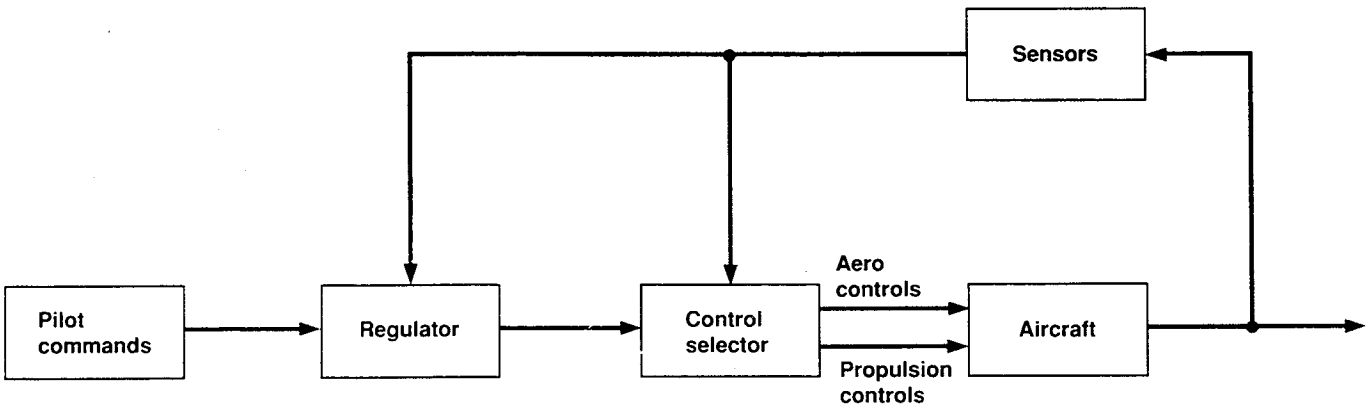

Figure 3. Flight-and-propulsion control system structure.

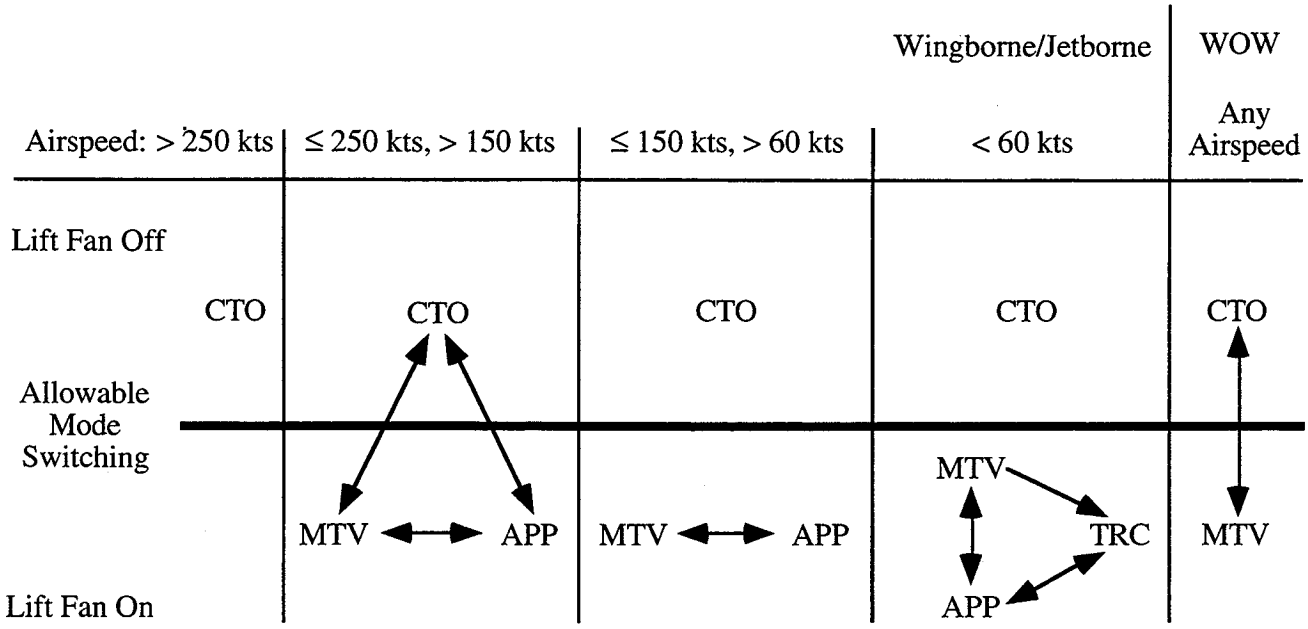

- When airborne/jetborne, the pilot cannot manually disengage the lift fan until the total thrust vector is deflected fully aft
- Disengagement of the nozzle lever clutch in APP or TRC mode causes reversion to the MTV mode
- Switching between FTM and ATM submodes within APP not shown as this change does not depend on airspeed

Figure 4. Control mode selection logic.

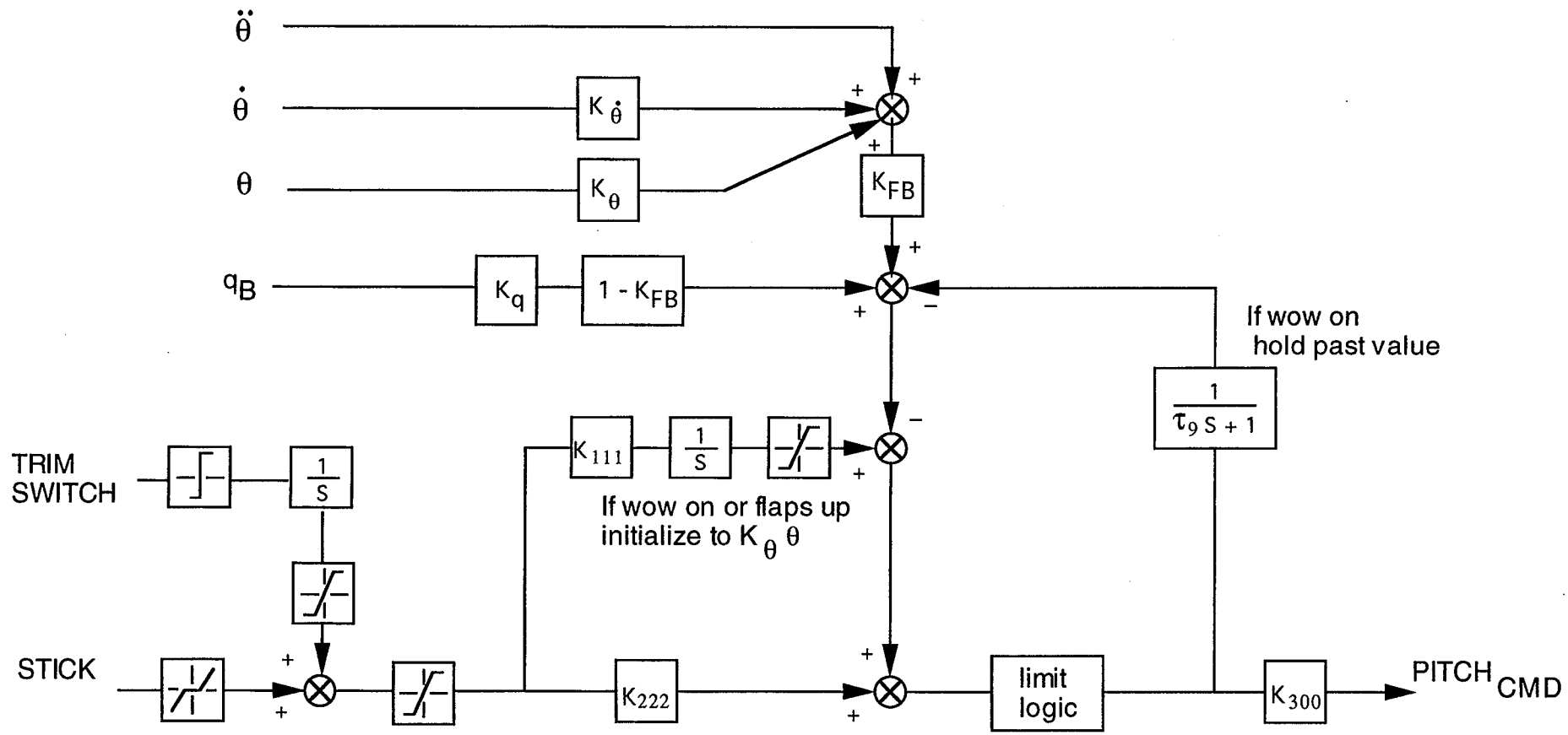

Figure 5. Pitch stabilization and command augmentation system.

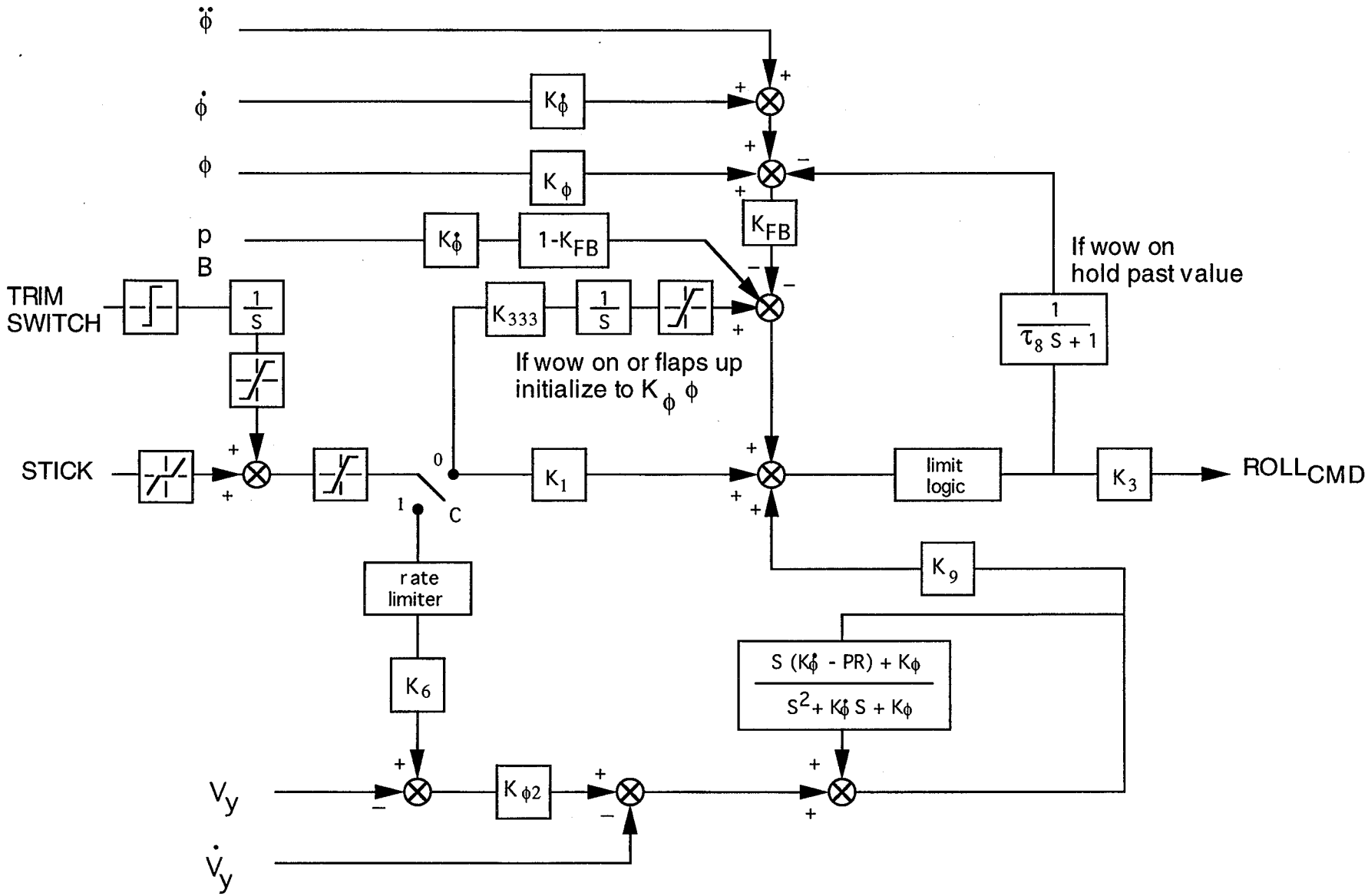

Figure 6. Roll stabilization and command augmentation system.

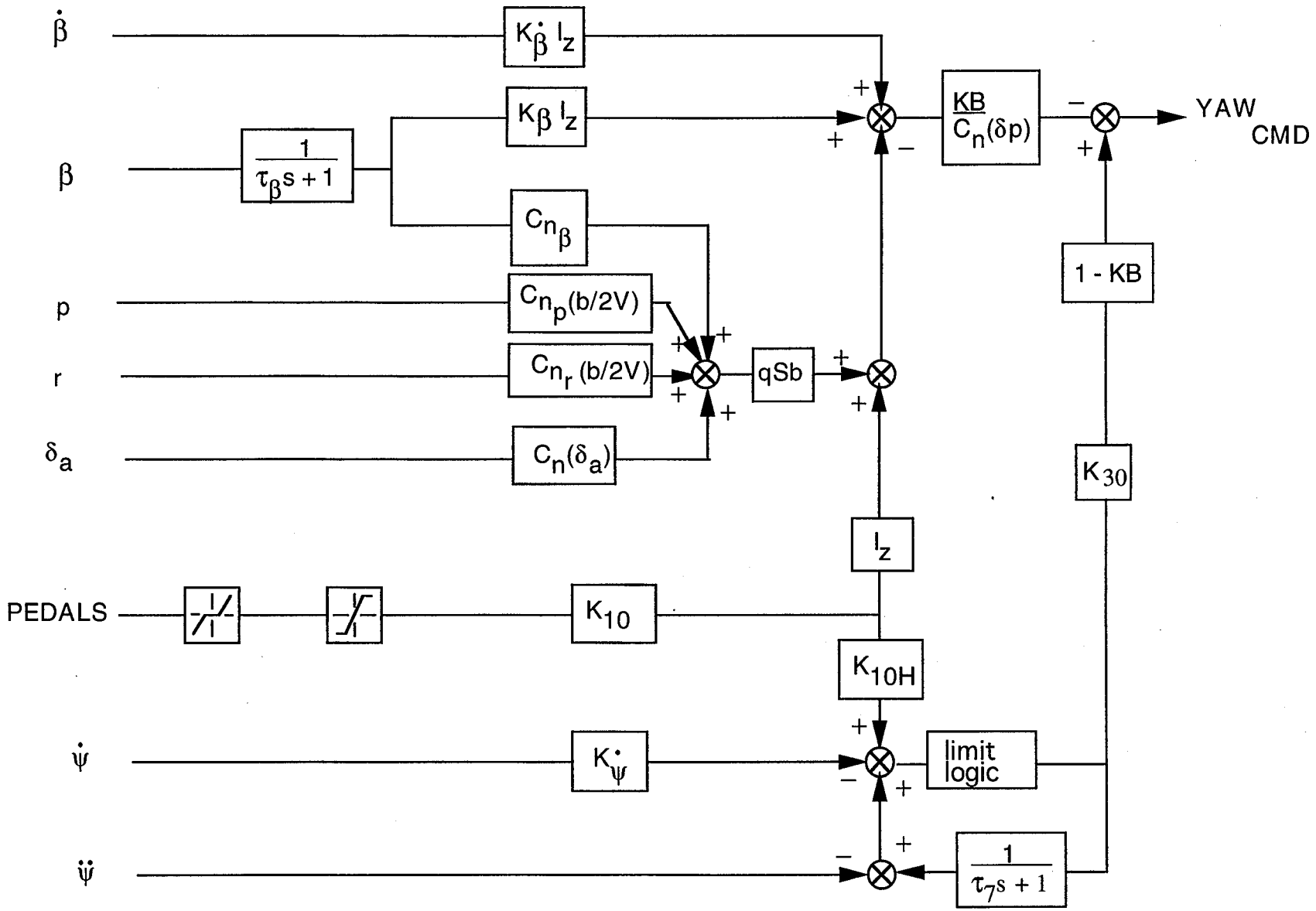

Figure 7. Yaw stabilization and command augmentation system.

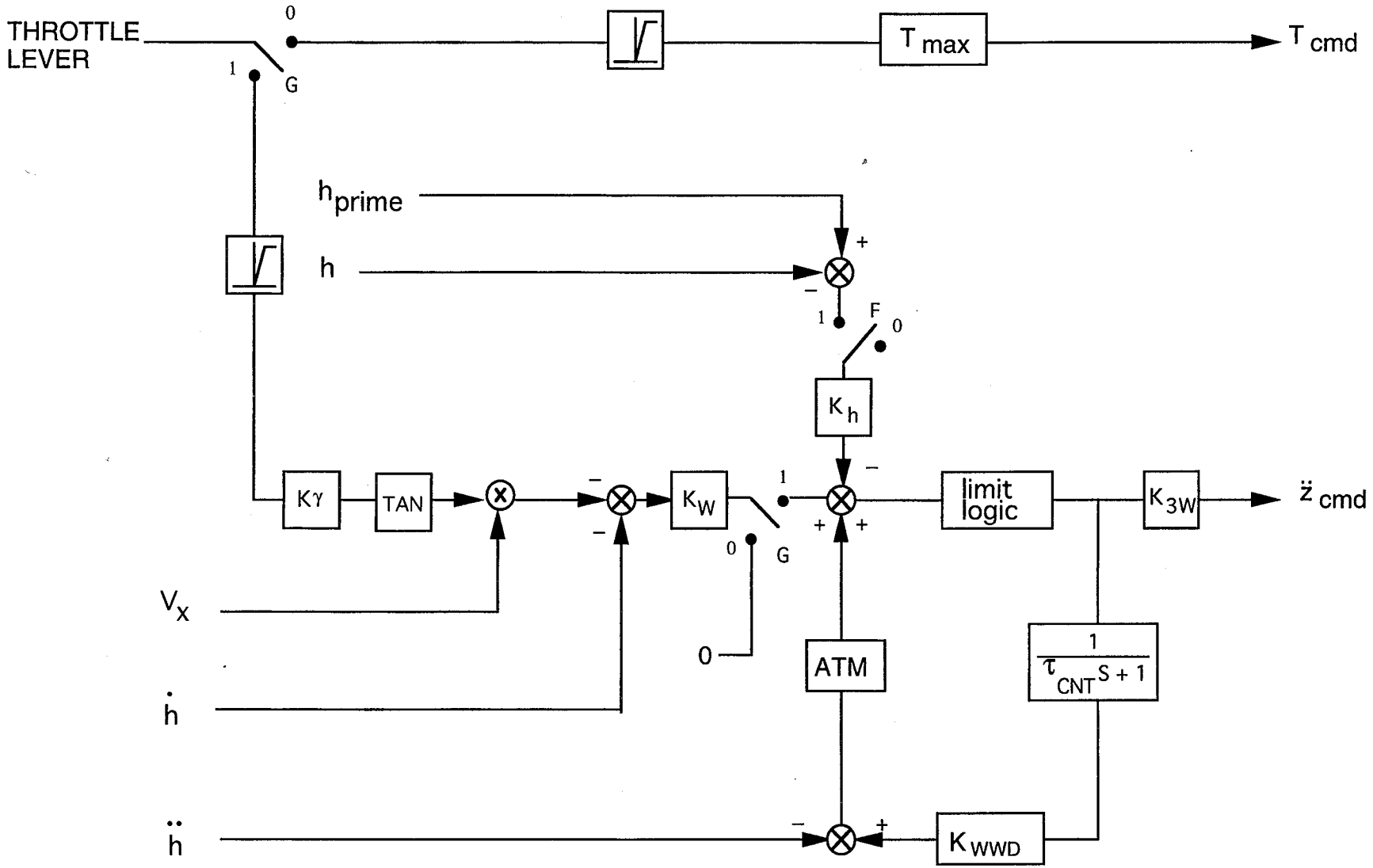

Figure 8. Vertical velocity stabilization and command augmentation system.

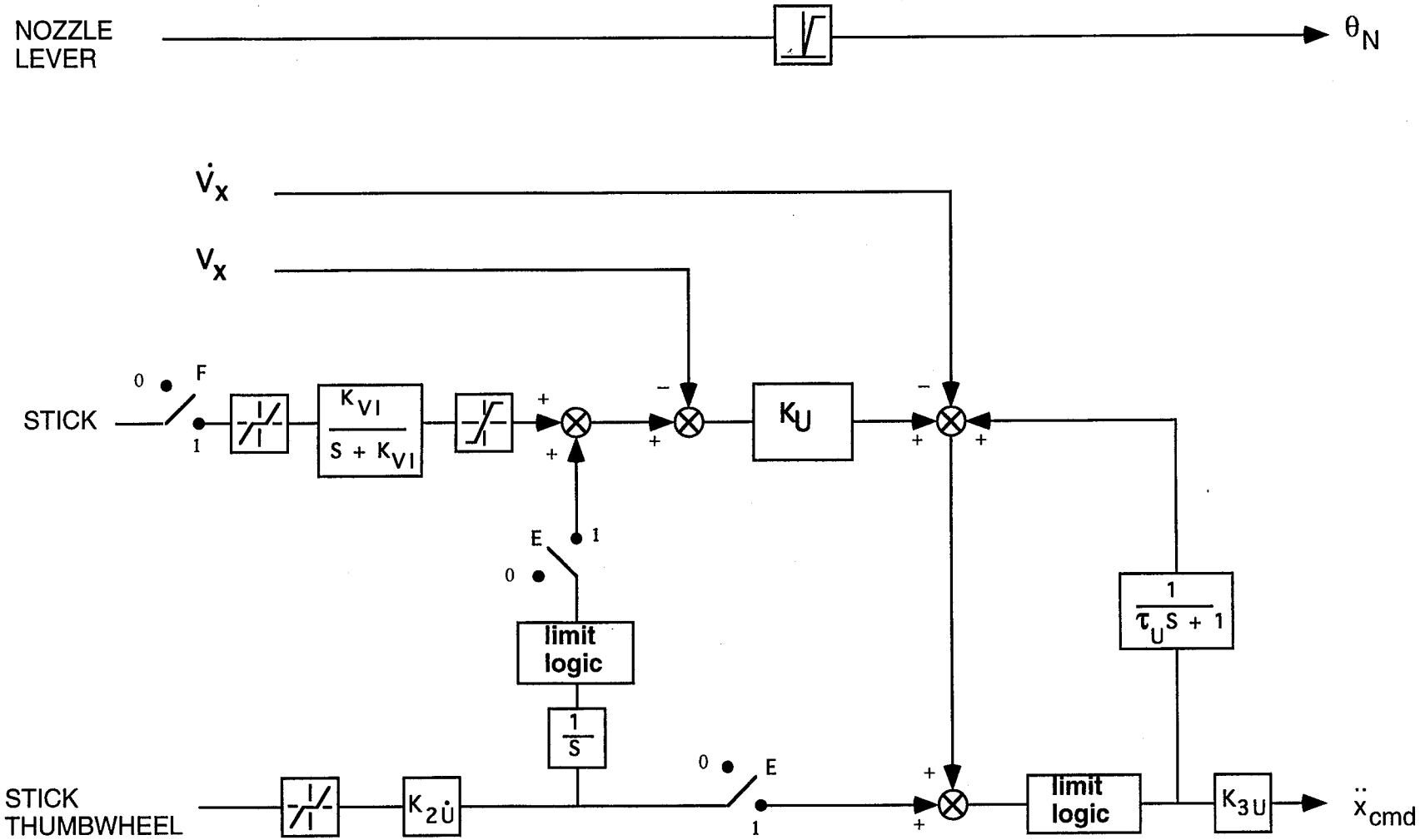

Figure 9. Longitudinal velocity stabilization and command augmentation system.

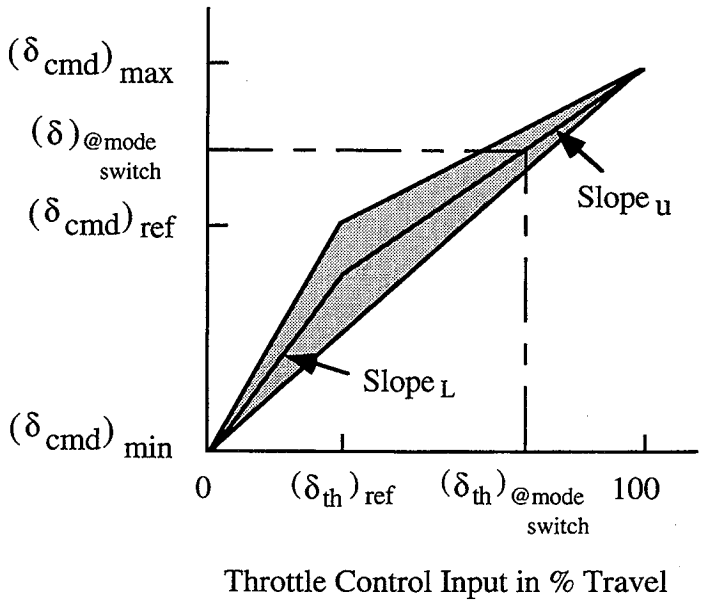

Figure 10. Throttle control/command scale.

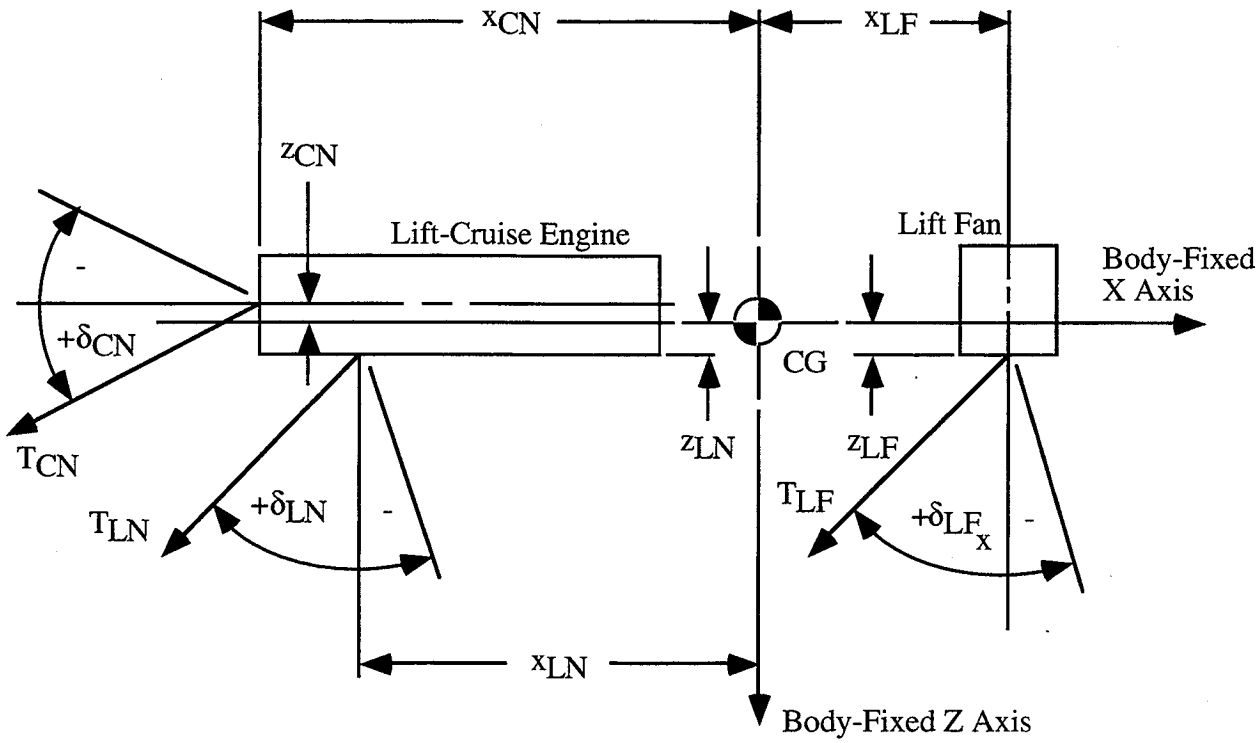

Note: Distances measured forward of the center of gravity are considered positive. Distances mesured below the center of gravity are considered positive.

x_{CN} = -19.72 ft

z_{CN} = 0 ft

x_{LF} = 11.70 ft

z_{LF} = 1.93 ft

x_{LN} = -8.93 ft

z_{LN} = 1.41 ft

δ_{CN} range = +20°, -20°

δ_{LF} range = +45°, -10°

δ_{LN} range = +45°, -10°

Figure 11. Propulsion system dimensions and sign conventions.

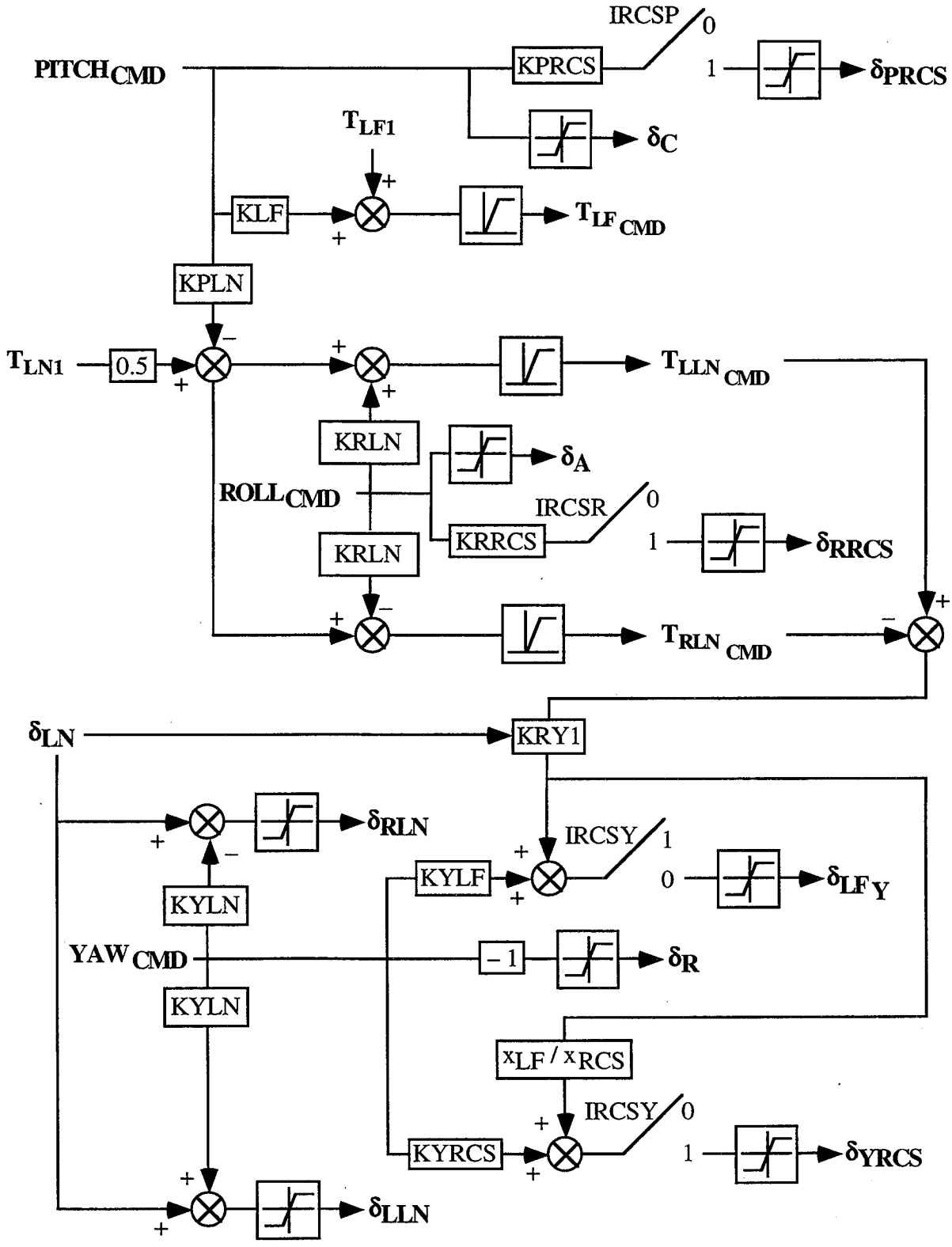

Figure 12. Control selector.

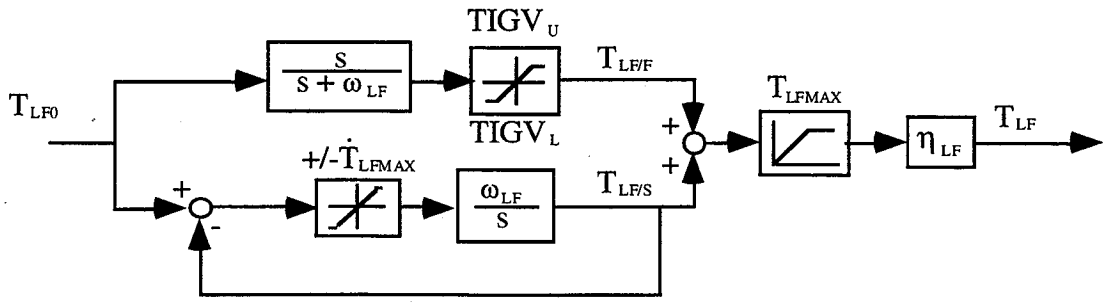

Figure 13. Lift fan inertia and IGV model.

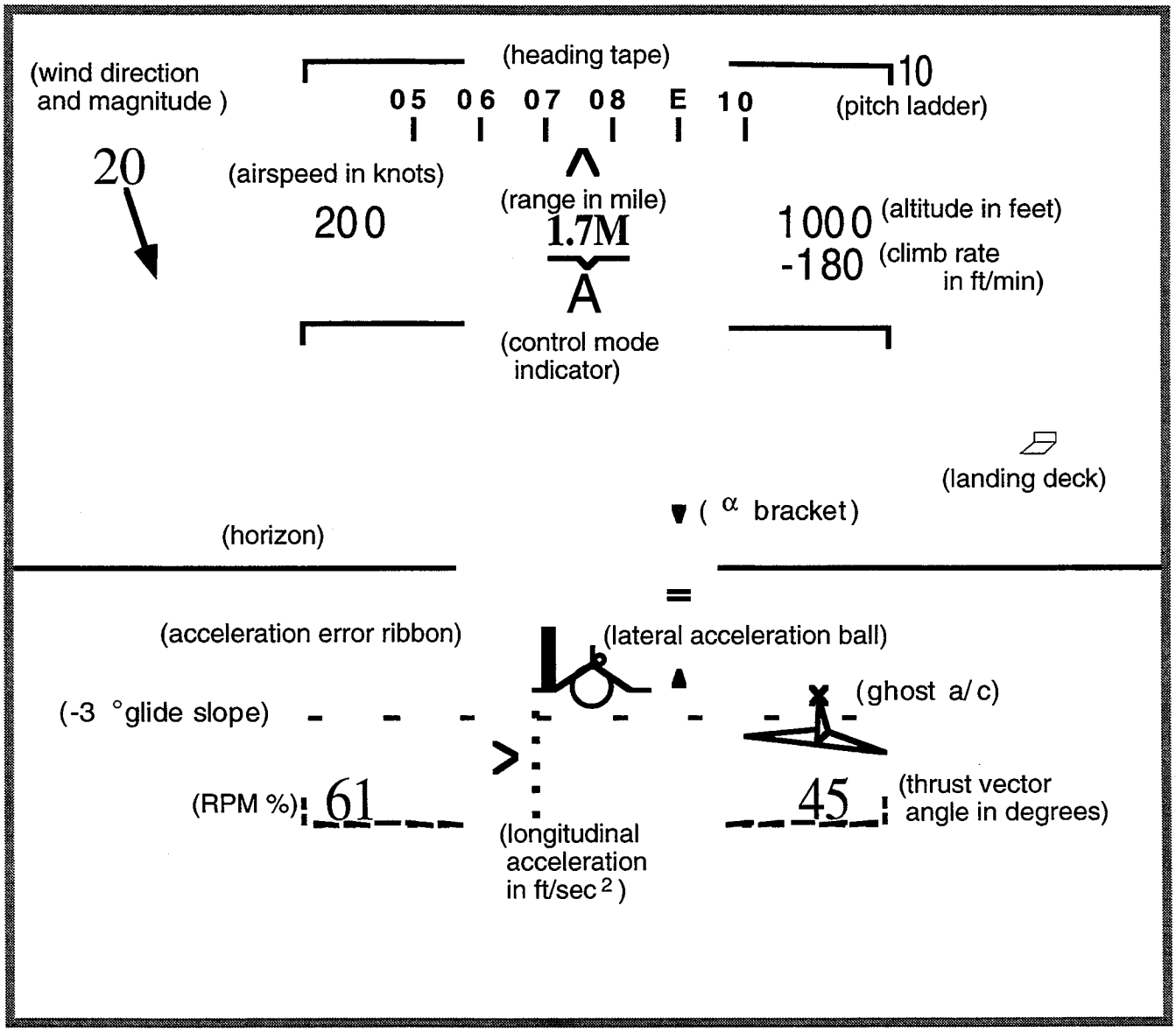

Figure 14. Head-up display approach mode.

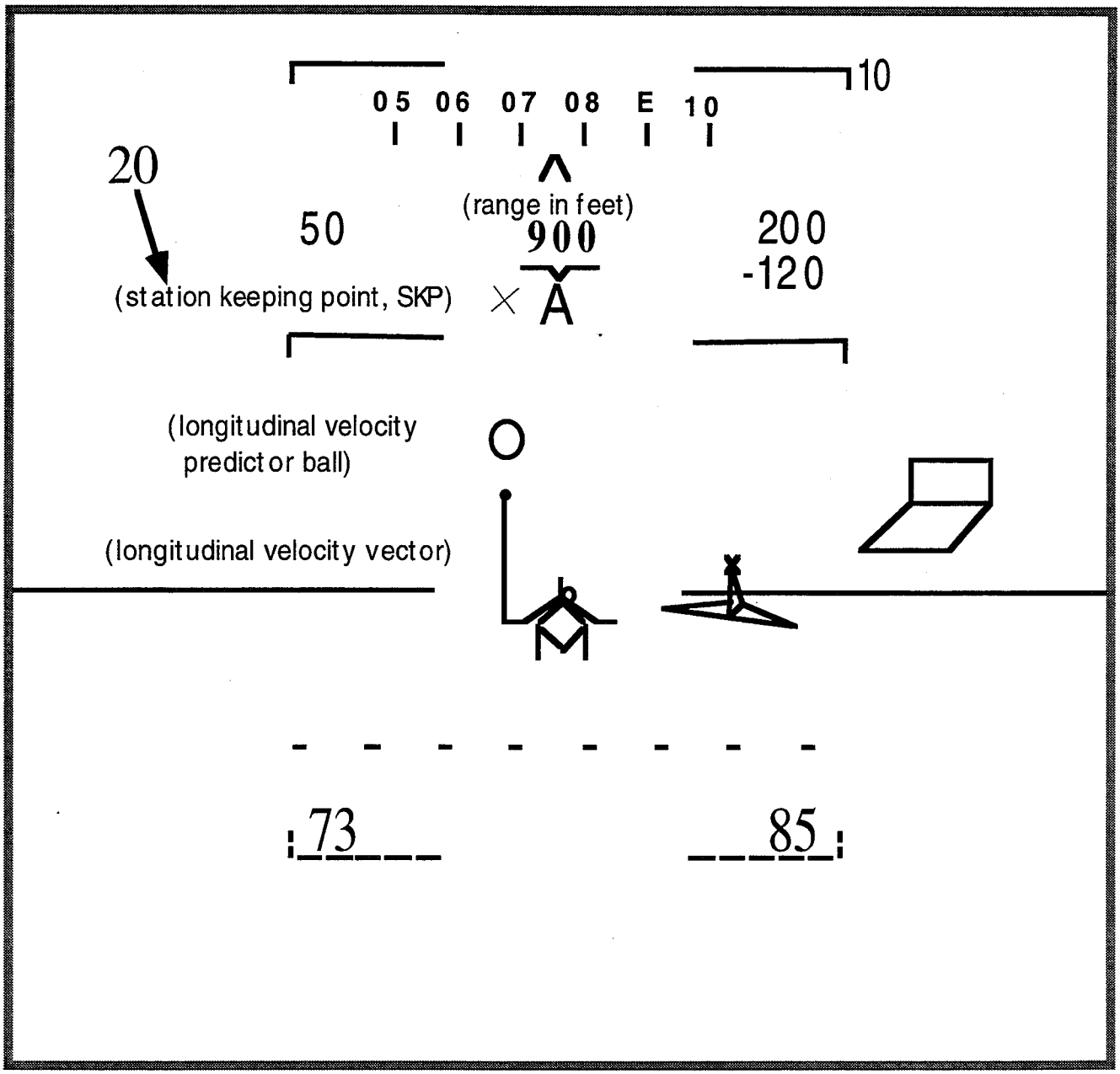

Figure 15. Head-up display approach mode for station keeping point capture.

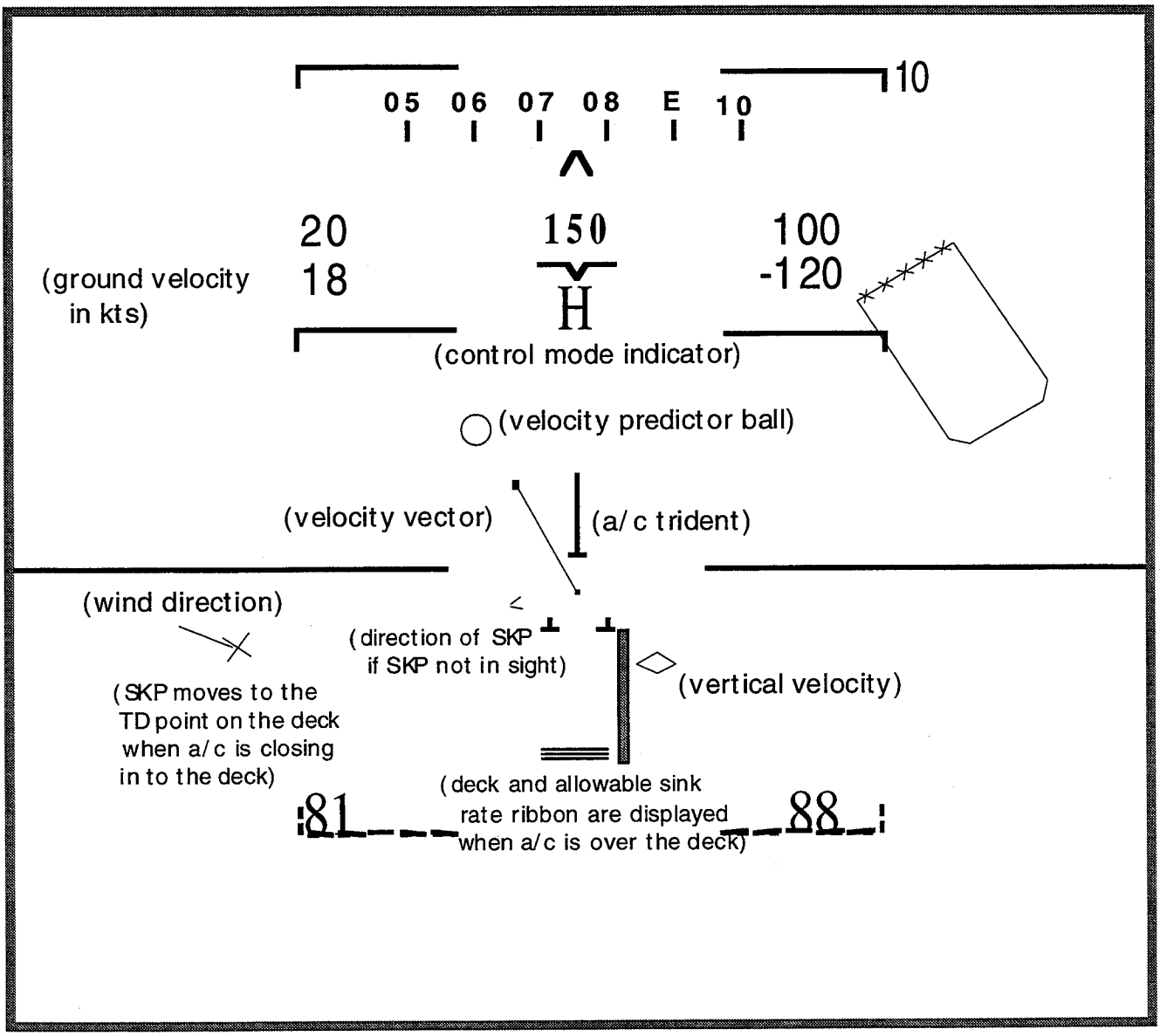

Figure 16. Head-up display hover mode.

REPORT DOCUMENTATION PAGE

Form Approved
OMB No. 0704-0188

1. AGENCY USE ONLY *(Leave blank)*	2. REPORT DATE	3. REPORT TYPE AND DATES COVERED
	April 1995	Technical Memorandum

4. TITLE AND SUBTITLE

Simulation Model of the Integrated Flight/Propulsion Control System, Displays, and Propulsion System for an ASTOVL Lift-Fan Aircraft

5. FUNDING NUMBERS

505-68-32

6. AUTHOR(S)

William W. Y. Chung, Paul F. Borchers, and James A. Franklin

7. PERFORMING ORGANIZATION NAME(S) AND ADDRESS(ES)

Ames Research Center
Moffett Field, CA 94035-1000

8. PERFORMING ORGANIZATION REPORT NUMBER

A-950048

9. SPONSORING/MONITORING AGENCY NAME(S) AND ADDRESS(ES)

National Aeronautics and Space Administration
Washington, DC 20546-0001

10. SPONSORING/MONITORING AGENCY REPORT NUMBER

NASA TM-108866

11. SUPPLEMENTARY NOTES

Point of Contact: Paul F. Borchers, Ames Research Center, MS 211-2, Moffett Field, CA 94035-1000; (415) 604-6115

12a. DISTRIBUTION/AVAILABILITY STATEMENT

Unclassified — Unlimited
Subject Category 05, 07, 08

12b. DISTRIBUTION CODE

13. ABSTRACT ***(Maximum 200 words)***

A simulation model has been developed for use in piloted evaluations of takeoff, transition, hover, and landing characteristics of an advanced, short takeoff, vertical landing lift fan fighter aircraft. The flight/propulsion control system includes modes for several response types which are coupled to the aircraft's aerodynamic and propulsion system effectors through a control selector tailored to the lift fan propulsion system. Head-up display modes for approach and hover, tailored to their corresponding control modes are provided in the simulation. Propulsion system components modeled include a remote lift and a lift/cruise engine. Their static performance and dynamic response are represented by the model. A separate report describes the subsonic, power-off aerodynamics and jet induced aerodynamics in hover and forward flight, including ground effects.

14. SUBJECT TERMS	15. NUMBER OF PAGES
STOVL, IFPCS (integrated flight/propulsion control system)	52
	16. PRICE CODE: A04

17. SECURITY CLASSIFICATION OF REPORT	18. SECURITY CLASSIFICATION OF THIS PAGE	19. SECURITY CLASSIFICATION OF ABSTRACT	20. LIMITATION OF ABSTRACT
Unclassified	Unclassified		